Title: Circadian ribosome profiling reveals a role for the *Period2* upstream opening reading frame in sleep

Arthur Millius[1,2,3], Rikuhiro Yamada[1], Hiroshi Fujishima[1], Kazuhiko Maeda[2], Daron M. Standley[3], Kenta Sumiyama[4], Dimitri Perrin[5], and Hiroki R. Ueda[1,6]

Affiliations

1) Laboratory for Synthetic Biology, RIKEN Quantitative Biology Center, Suita, Osaka, Japan
2) Laboratory for Host Defense, iFReC, Suita, Osaka, Japan
3) Laboratory for Systems Immunology, iFReC, Suita, Osaka, Japan
4) Laboratory for Mouse Genetic Engineering, RIKEN Center for Biodynamics Research, Suita, Osaka, Japan
5) School of Computer Science, Queensland University of Technology, Brisbane, Australia; Centre for Data Science, Queensland University of Technology, Brisbane, Australia
6) Department of Systems Pharmacology, Graduate School of Medicine, The University of Tokyo, Tokyo, Japan

Abstract

Many mammalian proteins have circadian cycles of production and degradation, but de novo transcription is only responsible for a small fraction of this rhythmicity. We used ribosome profiling to quantify RNA translation in liver from circadian-entrained mice transferred to constant darkness conditions over a 24-h period and compared translation levels to absolute protein production for 16 circadian proteins. We observed a delay between translation and peak protein levels for several circadian genes covering a wide range of translation efficiencies. We found extensive binding of ribosomes to upstream open reading frames (uORFs) in circadian mRNAs, including the core clock gene *Period2 (Per2)*. Increased uORFs in 5' UTRs was associated with decreased ribosome binding in downstream ORFs and reduced expression of synthetic reporter constructs in vitro and in single cells. Mutation of the *Per2* uORF increased luciferase and fluorescence reporter expression in 3T3 cells without altering phase or period. Genomic Per2 uORF mutation using CRISPR/Cas9 increased PER2 expression in PER2:Luc MEFs and reduced sleep in *Per2* uORF mutant mice. These results suggest that post-transcriptional processes shape translation of mRNA transcripts, which can impact physiological rhythms and sleep.

Introduction

Life is remarkably adapted to the 24-hour rotational movement of the earth. In mammals, the molecular time-keeping mechanism for circadian rhythms relies primarily on a hierarchical network of transcription activators and repressors in cells and tissues (Mohawk et al., 2012). In the past, circadian clocks have been measured using systems approaches to quantify genome-wide changes in RNA levels (Millius and Ueda, 2017), which has resulted in understanding the transcriptional regulatory network; however, less is known about how translation and post-transcriptional regulation influence biological rhythms.

Although 10% of genes are rhythmic in the liver (Akhtar et al., 2002), de novo transcription is only responsible for a small fraction of this rhythmicity (Koike et al., 2012). Thus, gene expression studies using microarrays and RNA-sequencing does not necessarily correlate with translation of the corresponding mRNA or with protein abundance (Gygi et al., 1999). Furthermore, proteomic studies have revealed a number of proteins with 24-h rhythms without a corresponding rhythmic RNA transcript (Lim and Allada, 2013; Reddy et al., 2006), which may suggest a role for translation in regulating the clock (Mauvoisin et al., 2014).

In mouse liver, detection of low-abundant components of the core circadian circuit using systems proteomics is difficult (Mauvoisin et al., 2014; Robles et al., 2014), unless special care is taken to examine a particular protein on a case-by-case basis (Narumi et al., 2016) or by other advances in mass-spectrometry (Robles et al., 2017; Wang et al., 2017). Researchers have used next-generation sequencing techniques of ribosome-bound mRNA protected from RNAse degradation (Ingolia et al. 2009) as a proxy for protein abundance and to understand how translation regulation affects protein abundance. Previous studies using ribosome profiling to measure daily rhythms used a cell culture model (Jang et al., 2015) or mouse tissues in light-dark (LD) conditions (Atger et al., 2015; Castelo-Szekely et al., 2017; Janich et al., 2015), which reflects diurnal gene expression affected by light cues. These studies also examined RNA expression to compare the timing between transcription and translation, but it remains unclear how translated RNA is converted into protein, both in terms of efficiency and timing. For example, production of PER and CRY proteins are delayed relative to expression of their mRNA in the liver (Lee et al., 2001) and SCN (Field et al., 2000). This difference in timing may result from a delay in RNA processing before translation, such as export from the nucleus or poly-adenylation, or a delay after translation, such as translation termination, protein folding, or degradation (Honkela et al., 2015; Liu et al., 2016).

Previously, we developed a mass spectrometry method called MS-based Quantification By isotope-labeled Cell-free products (MS-QBiC) to determine the absolute protein levels of 16 selected circadian proteins in mice liver over a 24-h period (Narumi et al., 2016). The method takes advantage of a reconstituted cell-free protein expression system termed the PURE system (Shimizu et al., 2001) to synthesize optimal peptide standards for detection and quantification using SRM-based targeted proteomics analysis. We found delays between the peak levels of RNA expression measured by quantitative PCR (qPCR) and the corresponding protein. Here, we investigated the same liver samples by ribosome profiling to understand the timing and efficiency of translation relative to RNA expression and protein production. We observed a longer delay between the peak of translation and that of protein production compared to the timing between transcription and translation. In addition, we found that upstream open reading frames (uORFs) disrupted translation globally, repressed reporter expression in a combinatorial manner, and disrupted production of PER2 protein using CRISPR/Cas9 homologous recombination. Mutation of the *Per2* uORF in mice reduced total sleep duration, particularly during the early morning and early evening, without disrupting the circadian period, which suggests that translational repression of uORFs may impact physiological behaviors.

Results

Ribosome profiling of liver from mice in constant darkness conditions

An experimental workflow was designed to analyze ribosome-protected mRNA fragments from liver samples previously examined by MS-QBiC (Narumi et al., 2016) (Fig. S1 and SI Results). Briefly, mice were entrained to a 12-h light/12-h dark (LD) cycle for 14 days, transferred to constant darkness for 24 h, and liver samples from two mice were collected and analyzed at circadian times (CT0, CT4, CT8, CT12, CT16, CT20, and CT24) according to established ribosome profiling protocols (Ingolia et al., 2012). We prepared ribosome profiling libraries and sequenced ~70 million reads per sample, which yielded 25-45 million reads mapped to mRNA (Table S1). Ribosome-protected fragments primarily aligned to the coding region and 5' untranslated region (5' UTR) of mRNA with few reads mapping to the 3' untranslated region (3'UTR) (Fig. S2A). Alignment of CDS-mapped reads based on the footprint length (see Methods) revealed reading frame periodicity (Fig. S2B). Reads were of the expected size (Fig. S2C), mapped with a high percentage to mRNA (Fig. S2D), and were correlated between samples (Fig. S2E).

From ~14,000 well-translated transcripts, defined by a median of at least two reads per five-codon mRNA window, we identified rhythms in ribosome-protected read fragments using the JTK_CYCLE algorithm (Hughes et al., 2010) and found 2952 rhythmic transcripts with an adjusted p-value < 0.05, which included well-known circadian transcripts such as *Bmal1, Per1, Per2, Clock,* and *Cry1* and 137 rhythmic transcripts with a BH.Q < 0.05 (Table S2; Fig S3).

Relationship between ribosome profiling reads and protein levels

We compared the timing of translation as measured by ribosome profiling reads to that of absolute protein molecules per cell for 16 previously reported core circadian proteins (Narumi et al., 2016). There was broad agreement in the timing of translation compared to that of protein synthesis (Fig. 1A). However, for several circadian proteins, such as BMAL1 and CLOCK, there was a delay of approximately 6 hours between translation and protein acrophases, clearly outside the 4-h range of our sampling intervals (Fig. 1B). We compared the average number of ribosome profiling reads to the number of protein molecules over a 24-h period, but found that the two values were poorly correlated (Fig. 1C). Thus, depending

on the protein, ribosome profiling reads may serve as a proxy for quantitative proteomics at individual time points, but post-transcriptional and post-translation mechanisms modulate peak protein production in non-uniform manner (Kojima et al., 2011).

Next, we investigated the efficiency of protein production based on ribosome profiling reads. For some proteins, such as BHLHE40, a large amount of translation resulted in a moderate amount of protein (Fig. 1D); whereas for other proteins, such as PER2, a much smaller amount of translation produced the same amount of protein as BHLHE40 (Fig. 1E). We examined the relationship between RNA transcription, as measured by qPCR (Narumi et al., 2016), and ribosome profiling reads, and observed a close agreement between the dynamics of transcription and translation (Fig. S4), as reported in other ribosome profiling studies of circadian transcripts in LD (Atger et al., 2015; Jang et al., 2015; Janich et al., 2015).

We compared the mRNA, ribosome profiling, and protein phases in our dataset in DD to previously published studies of mouse liver using ribosome profiling and mass spectrometry in LD (Atger et al., 2015; Jang et al., 2015; Janich et al., 2015; Wang et al., 2017), and observed a correlation with an approximately 1-2 h delay in the phases in DD (Fig. S5A, C). The transcripts with the largest differences in delay in mRNA-to-protein production between LD and DD conditions included *Nfil3*, *Per2*, *Per3*, and *Bmal1* (Fig. S5B) resulting from a slightly earlier peak in the amount of RNA in LD rather than a later peak in the amount of protein, and little difference in delay in transcription and translation between LD and DD (Fig. S5D).

Upstream open reading frames (uORFs) suppress translation

We also noticed a relationship between ribosome occupancy and upstream open reading frames (uORFs), similar to previous reports (Jang et al., 2015; Janich et al., 2015). In particular, for circadian transcripts, such as *Cry1* and *Bmal1*, there appeared to be increased ribosome binding in uORF regions, as measured by increased ribosome profiling reads (Fig. 2A), although ribosome binding in the 5'UTR was not necessarily associated with uORFs in circadian transcripts (Fig. S6A). Roughly half of all mouse transcripts contained at least one uORF (Fig. S6B). mRNAs with increased numbers of uORFs had lower levels of ribosome occupancy in the downstream coding region (Fig. 2B), whereas the length of the uORF and the distance of the uORF to the start codon did not have a significant impact on ribosome binding in the downstream coding region (Fig. S6C, D). To investigate whether uORFs were

sufficient to suppress translation in a combinatorial manner, we created a luciferase reporter vector with multiple synthetic uORFs. Predictably, increasing the number of uORFs reduced luminescence from the reporter (Fig. 2C). Using our synthetic reporter, we varied the position of a single uORF relative to the start codon or its length and found a higher degree of uORF-mediated repression the closer the uORF to the start codon, but no effect from uORF length (Fig. S6E, F). Other factors, such as Kozak consensus of the uORF, overlap with the CDS, and conservation may also impact repression strength (Chew et al., 2016; Johnstone et al., 2016).

The Per2 uORF suppresses reporter expression without altering phase or period

To further explore the impact of uORFs on circadian translation, we focused on the uORF in the circadian transcript *Per2*. This uORF is evolutionarily conserved and short (Fig. 3A), which eliminates any potential effect of translated uORF peptide on the regulation of *Per2*. Mutation of the uORF in *Per2* increased the amplitude of expression without affecting the phase or period (Fig. 3B, C). This increase in amplitude was not affected by the amount of transfected plasmid, inclusion of the full-length Per2 5'UTR, or addition of PER2 protein (Fig. S7). CRISPR/Cas9-mediated mutation of the *Per2* uORF in PER::LUC MEFs also increased the amplitude of luciferase expression (Fig. 3D).

To understand how these amplitude differences affect individual cells, we created green and red fluorescent reporters driven by the *Per2* promoter with or without a mutation in the *Per2* uORF. We transfected 3T3 cells with different combinations of the uORF reporters and analyzed the cells by FACS and fluorescence microscopy. Mutation of the uORF increased both the total number of red- or green-expressing cells (Fig. 3E) and the brightness of individual cells (Fig. 3F, G), although the level of fluorescence and amount of uORF repression varied between cells, consistent with intrinsic noise in RNA translation (Dacheux et al., 2017). Thus, the *Per2* uORF variably repressed translation of mRNA transcripts within individual cells to control circadian amplitude.

Mice with a mutation in the Per2 uORF have reduced sleep

We used CRISPR/Cas9 to generate a knock-in mouse harboring a mutation in the uORF of *Per2*, which removed both the start and stop codon of the uORF without disrupting the nearby E'-box (Fig. S8). Mice were phenotyped over 13 days in 12-h light/12-h dark (LD) conditions and then for 12 days in constant darkness conditions (DD) using the Snappy Sleep

Stager (Sunagawa et al., 2016; Tatsuki et al., 2016), which is a respiration-based method to characterize sleep/wake parameters and circadian rhythms. Both male and female *Per2* uORF mutant mice had significantly reduced sleep per day (mean ± SEM: 717 ± 19 min and 642 ± 7 min, respectively) compared to that of wild-type littermates (774 ± 11 min and 678 ± 4 min, respectively, $P < 0.001$ by two-way ANOVA), and a corresponding increase in wake duration per day (Fig. 4A, B and Fig. S9A). There was a decrease in sleep episode duration and a significant increase in the transition probability from sleep to awake termed P_{sw} in *Per2* uORF mutant mice (Fig. S9B), but there were no differences in other sleep parameters such as amplitude, P_{ws} (the transition probability from awake to sleep), or wake episode duration (Fig. S9C). *Per2* uORF mutant mice exhibited reduced sleep duration particularly during the light-to-dark and dark-to-light transitions in the early morning and early evening (Fig. 4C, D). There were also differences in sleep duration later in the morning (Fig. S9D), but not at other times during the day (Fig. S9E). Next, we observed mice in constant darkness over 12 days and found no differences in activity rhythms and period (Fig. 4E); consistently, cosinor analysis of the activity rhythms in light-dark or constant darkness conditions revealed no differences in period and amplitude between wild-type and *Per2* uORF mutant mice (Fig. S10). Taken together, these results suggest that *Per2* expression is regulated by the *Per2* uORF, which has a significant impact on sleep duration.

Discussion

Global proteomics studies of mice livers revealed large numbers of diurnally rhythmic proteins and estimated that 20–50% may be dependent on post-transcriptional and post-translational mechanisms (Mauvoisin et al., 2014; Robles et al., 2014, 2017; Wang et al., 2017, 2018). Previously, we used targeted proteomics to detect the rhythmicity and concentration of a select number of low abundant core circadian proteins in constant darkness conditions (Narumi et al., 2016). Here, we used ribosome profiling and quantitative mass spectrometry to understand the relationship between those circadian protein rhythms and mRNA translation.

We focused on the timing and abundance of 16 core circadian proteins and found a correlation in the timing of translation and peak protein abundance for most transcripts (Fig. 1), which suggests that ribosome profiling can provide an approximate estimate for when a protein is produced. However, for BMAL1 and CLOCK protein, although there was a close relationship between the transcription and translation (Fig. S4), there was a delay between translation and protein synthesis (Fig. 1). This delay is thus likely caused by changes in protein stability—including phosphorylation, SUMOylation, and deacetylation (Okamoto-Uchida et al., 2019)—rather than mRNA stability or translation. Previous studies have found that the peak protein abundance of PER and CRY is slightly delayed relative to their peak mRNA abundance (Field et al., 2000; Lee et al., 2001; Narumi et al., 2016). We found that this delay occurs after translation and not by a delay between transcription and translation (Fig. S4), similar to previous ribosome profiling studies (Atger et al., 2015; Jang et al., 2015; Janich et al., 2015). There was a larger delay between peak abundance of *Cry2* mRNA and CRY2 protein than that of *Cry1*, which may simply be a result of the lower amplitude of CRY2 rhythms.

Most transcripts with rhythmic translation in our dataset had a phase around CT00 corresponding to what would be the dark-to-light transition (Fig. S3). Less than 10% of the circadian translatome had significantly rhythmic mRNA transcription according to JTK cycle analysis ($P < 0.05$), and these transcripts were enriched for circadian and metabolic processes by Panther gene ontology (GO) analysis (Fig. S3B, C). Transcripts with a non-significant mRNA rhythmicity by JTK cycle analysis ($P > 0.05$) also were biased toward CT00, but there was no clear GO biological process underlying these rhythms (Fig. S3D, E). The set of transcripts with phases between CT22 and CT02 (Fig. S3F, G) included *Npas2*, *Bmal1*, *Cry1*,

Nfil3, and *Clock* are all regulated by the nuclear receptor NR1D1, also known as Rev-erbα, which transcriptionally represses many genes involved in metabolism in a tissue- and circadian-dependent manner (Everett and Lazar, 2014). In the liver, NR1D1 predominantly binds genomic locations at ZT08-ZT10 with little-to-no binding at ZT22 (Feng et al., 2011; Hunter et al., 2020; Zhang et al., 2015). Thus, NR1D1 de-repression may be driving the transcriptional and subsequent translational peak observed in our data between CT22 and CT02 and may indirectly account for the translation peaks observed in mRNA non-rhythmic transcripts.

We observed widespread binding of ribosomes to uORFs in the 5'UTRs of many core circadian transcripts and found an inverse relationship between uORF number and ribosome occupancy or luciferase expression in transiently transfected reporters and CRISPR/Cas9-generated MEF cells (Fig. 2 and Fig. S6). Approximately 50% of mouse and human mRNAs contain uORFs, and uORFs are associated with widespread translational repression (Johnstone et al., 2016). Thus, uORF translation suppression may constitutively lower the abundance of circadian proteins or provide a post-transcriptional foothold to adjust protein abundance by altering the activities of ribosome reinitiation factors (Bohlen et al., 2020; Morris and Geballe, 2000; Schleich et al., 2014), and mutagenesis of uORFs have been shown to alter rhythmicity in other circadian systems (Diernfellner et al., 2005; Wu et al., 2022)

The uORF in the *Per2* 5'UTR is an attractive target to understand the role of uORFs in circadian biology, not only because cis-elements within the *Per2* promoter are well-understood (Doi et al., 2019; Gekakis et al., 1998; Hao et al., 1997; Ueda et al., 2005), but also because the *Per2* uORF is too short to encode a peptide. PER2 production is post-transcriptionally controlled by miRNAs (Park et al., 2020; Yoo et al., 2017), antisense transcription (Mosig et al., 2021), and hnRNP1-mediated mRNA degradation (Woo et al., 2009), which suggests that *Per2* post-transcriptional control is important for producing the correct amount of PER2 protein. Mutation of the *Per2* uORF increased amplitude without affecting period or phase (Fig. 3), similar to effects observed by mutating the Per2 antisense transcript (Mosig et al., 2020). Taken together, uORFs are one marker of post-transcriptional control of protein production in circadian proteins.

Both abundance and timing of *Per2* expression are critical for maintaining circadian rhythmicity in mice because constitutive expression of PER2, unlike CRY1, disrupts behavioral rhythms (Chen et al., 2009). Several post-transcriptional mechanisms such as *Per2* anti-sense transcription (Mosig et al., 2021) and miRNAs (Nagel et al., 2009; Park et al., 2020; Yoo et al., 2017) in the *Per2* genomic locus alter the timing and abundance of PER2 protein expression. For example, replacing the *Per2* 3'UTR with a SV40 late poly(A) signal greatly amplifies bioluminescence rhythms in Per2:Luc mice and increases free-running periods (Yoo et al., 2017). By contrast, mutation of the *Per2* uORF resulted in a smaller increase in luminescence amplitude and period in cells (Fig. 3) and did not increase the free-running period in mice (Fig. 4). *Per2* uORF mutant mice did have reduced total sleep, as observed in *Per1/Per2* double mutant mice under similar sleep phenotyping conditions (Sunagawa et al., 2016). A slightly lower sleep episode duration and increase transition probability from sleep to wake contributed to the reduced sleep in *Per2* uORF mutant mice (Fig. S9b), and sleep was particularly reduced during light-to-dark and dark-to-light transitions (Fig. 4). Disruption of the E' box cis-element in the 5' genomic region of *Per2*, which is only a few base pairs upstream of the *Per2* uORF, abolishes molecular oscillations in mutant cells without disrupting the free running period in mice (Doi et al., 2019). These mice more quickly re-entrain under an artificial jetlag experiment than wild-type mice, and it will be interesting to observe how *Per2* uORF mutant mice behave under similar conditions. At a molecular level, de-repressed *Per2* translation in the absence of the *Per2* uORF may alter the timing and abundance of PER2 protein leading to a reduction in sleep, but further studies are needed to understand the precise mechanism by which sleep is reduced in these animals.

Methods

Animals. All animal experiments were approved by the Institutional Animal Care and Use Committee of the RIKEN Kobe branch. Eight-to-ten week-old wild-type male mice (C57BL/6N, Japan SLC) were entrained under 12-h light (400 lx) 12-h dark (LD) for two weeks. Twenty-four hours after transferring to constant darkness (DD), wild-type mice were sacrificed every 4 h over one day (CT0, CT4, CT8, CT12, CT16, CT20, and CT24) for ribosome profiling analysis as in (Narumi et al., 2016). Livers were excised, snap frozen in liquid nitrogen, and stored at -80 °C until use. *Per2* uORF mutant (uORF: ATGTGA to mutant uORF: GTAGGT) mice were generated by one-cell embryo microinjection of synthesized Cas9 mRNA, gRNA (5'-TTTCCACTATGTGACAGCGGAGG-3'), and ssODN (5'-GTCACGTTTTCCACTGTAGGTCAGCGGAGGGCGACG-3') in C57BL/6N fertilized eggs, and genotypes were confirmed by Sanger sequencing.

Plasmids. The pGL3-P(*Per2*)-d*Luc* reporter plasmid (Sato et al., 2006) was modified by standard PCR mutagenesis to generate pGL3-P(*Per2*)-uORF-d*Luc* (ATG->TTG mutation in the *Per2* uORF). Synthetic oligonucleotide linkers containing 0-4 artificial uORFs (Fastmac, Japan) were inserted into a PCR-linearized pGL3-P(*Per2*)-d*Luc* by In-Fusion cloning enzyme (Takara Bio). Plasmids containing full-length *Per2* 5'UTR and PER2 were cloned from mouse cDNA (Clone PX00938 H17, RIKEN) and pMU2-PER2-Luc (Isojima et al., 2009), respectively, and inserted into pGL3-P(*Per2*)-d*Luc* or pGL3-P(*Per2*)-uORF-d*Luc* by In-Fusion cloning to create pGL3-P(*Per2*)-5'UTR-d*Luc* and pGL3-P(*Per2*)-5'UTR-PER2-d*Luc* and the respective uORF mutant plasmids. Oligos for *Per2* sgRNA (5'-caccgTTCCACTATGTGACAGCGGA and 5'-aaacTCCGCTGTCACATAGTGGAAc) were annealed and inserted into *Bbs*I-digested pSpCas9(BB)-2A-Puro (Addgene #62988) or pSpCas9n(BB)-2A-Puro (Addgene #62987) to make pCas9-Per2 or pCas9n-Per2, respectively. The promoter sequences from pGL3-P(*Per2*)-d*Luc* or pGL3-P(*Per2*)-uORF-d*Luc* were cloned into pD1EGFP-N1 (Takara Bio) to create pD1-P(*Per2*)-EGFP or pD1-P(*Per2*)-uORF-EGFP, respectively. mCherry was PCR-amplified and blunt-end ligated into inverse-PCR amplified pD1-P(*Per2*)-EGFP or pD1-P(*Per2*)-uORF-EGFP for the mCherry versions. All plasmid sequences were verified by Sanger sequencing.

Ribosome Profiling. Ribosome profiling was performed essentially as described in (Ingolia et al., 2012). Frozen liver samples (~50 mg) were pulverized and then homogenized in 400 µl polysome lysis buffer (150 mM NaCl, 20 mM Tris-HCl pH 7.4, 5 mM $MgCl_2$, 5 mM DTT,

100 µg/ml cycloheximide, 1% Triton X-100, 25 U/ml Turbo DNAse I). Lysates were incubated on ice for 5-10 min, triturated through a 26-G needle 10 times, clarified by centrifugation (20,000 × *g* for 10 min at 4 °C), and 300 µl of supernatant was transferred to a new tube. Unbound RNA was digested by the addition of 7.5 µl RNAse I (ThermoFisher) for 45 min and then stopped by 10 µl SUPERase In RNAse Inhibitor (ThermoFisher). The digestion was transferred to 13 mm × 51 mm polycarbonate ultracentrifuge tubes, layered on top of 0.9 ml sucrose cushion (150 mM NaCl, 20 mM Tris-HCl pH 7.4, 5 mM $MgCl_2$, 5 mM DTT, 100 µg/ml cycloheximide, 1 M sucrose, 10 U/ml SUPERase In), centrifuged in a TLA100.3 rotor at 70,000 rpm at 4 °C for 4 h. Ribosome pellets were resuspended in 0.7 ml Qiazol and mRNA was recovered using the miRNeasy RNA extraction kit (Qiagen) according to the manufacturer's instructions. RNA was precipitated from the elution by the addition of 38.5 µl water, 1.5 µl GlycoBlue (ThermoFisher), and 10 µl 3 M sodium acetate pH 5.5 followed by 150 µl isopropanol, stored overnight at -80 °C, pelleted by centrifugation (20,000 × *g* for 30 min at 4 °C), and resuspended in 5 µl 10 mM Tris pH 8. Approximately 2–4 µg RNA was separated on a 15% (wt/vol) polyacrylamide TBE-urea gel at 200 V for 65 min in 1× TBE, and fragments between 26 and 34 nt were excised and recovered in 400 µl RNA gel extraction buffer (300 mM sodium acetate pH 5.5, 1 mM EDTA, and 0.25% (wt/vol) SDS) overnight. RNA was precipitated by the addition of 1.5 µl GlycoBlue and 500 µl, stored at -80 °C for >30 min, pelleted by centrifugation (20,000 × *g* for 30 min at 4 °C), and resuspended in 10 µl 10 mM Tris pH 8. RNA was dephosphorylated by T4 PNK (Takara Bio), precipitated and recovered as previously described, resuspended in 8.5 µl 10 mM Tris, and 1.5 µl of preadenylated and 3' blocked miRNA cloning linker (1/5rApp/CTGTAGGCACCATCAAT/3ddC/, IDT) was added. The linker mixture was denatured for 90 s at 80 °C, cooled to room temperature, ligated by T4 Rnl2 (NEB) for ~5 h at room temperature, precipitated, recovered, and separated by 15% TBE-urea gel electrophoresis. Ligation products were recovered overnight in RNA gel extraction buffer, precipitated, and recovered in 10 µl 10 mM Tris pH 8. Ligated RNA was reverse transcribed at 48 °C for 30 min using SuperScript III (ThermoFisher) with the reverse transcription primer (5′-(Phos)-AGATCGGAAGAGCGTCGTGTAGGGAAAGAGTGTAGATCTCGGTGGTCGC-(SpC18)-CACTCA-(SpC18)- TTCAGACGTGTGCTCTTCCGATCTATTGATGGTGCCTACAG-3′, where SpC18 indicates a hexa-ethyleneglycol spacer). Reverse transcription products were precipitated, recovered, separated by 15% TBE-urea gel electrophoresis, and recovered

overnight in DNA gel extraction buffer (300 mM NaCl, 10 mM Tris pH 8, and 1 mM EDTA). The cDNA was precipitated, recovered, resuspended in 15 µl 10 mM Tris pH 8, and circularized by CircLigase (EpiCentre) for 1 h at 60 °C. rRNA was depleted by combining 5 µl circularization reaction with 1 µl of subtraction oligo pool, 1 µl 20× SSC, and 3 µl water, incubating at 37 °C for 15 min and binding to MyOne Streptavidin C1 DynaBeads (ThermoFisher) at 37 °C for 15 min with mixing at 1000 rpm. Eluate was precipitated, recovered, and resuspended in 5 µl 10 mM Tris pH 8. rRNA-depleted cDNA was PCR amplified by Phusion High-Fidelity DNA Polymerase (NEB) in a 20 µl reaction (denature 94 °C for 15 s, anneal 55 °C for 10 s, extend 72 °C for 10 s) for 12-16 cycles. PCR products were separated on a 8% TBE gel, recovered overnight in DNA gel extraction buffer, precipitated, recovered, and resuspended in 15 µl 10 mM Tris pH 8. Libraries were quantified using the high-sensitivity DNA chip on the Agilent BioAnalyzer according to the manufacturer's protocol, pooled, and amplified on the Illumina HiSeq system according to the manufacturer's protocol.

Bioinformatic analysis of ribosome profiling. After quality control using FASTQC (https://www.bioinformatics.babraham.ac.uk/projects/fastqc/), reads were clipped using fastx_clipper (with parameters `-Q33 -a CTGTAGGCACCATCAAT -l 25 -c -n`) and processed with fastx_trimmer (with parameters `-Q33 -f 2`), both from the FASTX-Toolkit (http://hannonlab.cshl.edu/fastx_toolkit/). We then used Bowtie 2.1.0.0 (Langmead and Salzberg, 2012) to map the resulting reads to rRNA sequences. Reads that were successfully aligned to these sequences are discarded, and only unaligned reads were used for downstream analysis. These reads that did not align to rRNA were mapped to the mouse mm10 reference genome. Using samtools 0.1.19.0 and egrep, we extracted reads for which an exact match between the sequence and the reference could be found.

Using reads aligned to a unique location, we then calculated transcript density profiles. This relies on assignment each footprint alignment (i.e., each read) to a specific A site nucleotide based on the length of the fragment. The initial assumption is that this site will be close to the center of the read. To calculate the best offset, we considered a metagene that captured all reads and their position relative to the start site and calculated the offset that optimized phasing. The best results were obtained when the offset from the 5' end of the alignment was: 26 nt long, +13; 27-28 nt long, +15; 29-30 nt long, +16; 31-32 nt long, +17. Reads shorter than 26 or longer than 32 nucleotides were discarded. Using this offset, we assigned each

read to a unique nucleotide, and constructed transcript density profiles by counting the number of reads whose A site was assigned to each nucleotide position.

For each transcript, non-overlapping five-codon windows were then tiled across the coding region and the transcript was considered well-translated if it had a median value of at least 2 reads per window (excluding the excluding the first fifteen and the last five codons).

Using all well-translated transcripts, we created file where each transcript is represented across all samples by its RPKM value. We used this file in JTK_CYCLE (Hughes et al., 2010) to identify all rhythmic transcripts with a circadian period (i.e., period between 20 and 28 h). We used a threshold of 0.05 on the adjusted p-value to assess significance.

To detect uORFs, we processed the 5'UTR of all transcripts, extracted their sequence, and identified all pairs of a start codon and a stop codon in phase with each other. Using the same read assignment method as above, we also allocated reads aligned to the UTR to their corresponding uORF (where appropriate).

Cell culture. NIH3T3 and MEFs from PER2::LUCIFERASE (PER2::LUC) knock-in reporter mice (Yoo et al., 2004) were cultured in DMEM (ThermoFisher), 10% FBS (JRH Biosciences), and 1% penicillin/streptomycin (ThermoFisher) at 37 °C in 5% CO_2. PER2::LUC MEFs were plated in 10 cm dishes at a density 4×10^5 per well, transfected the next day with pCas9-Per2 or pCas9n-Per2 and 560 bp of single-stranded linearized DNA (Guide-it Long ssDNA Production System, Takara Bio) containing mutations in the Per2 uORF (ATGTGA->GTAGGT), and after 48-h selected in 1 µg/ml puromycin for puromycin-resistant clones according to (Ran et al., 2013). Individual clones were expanded, sequence-verified, and clones containing mutations in the Per2 uORF were used for downstream analysis.

Real-time Circadian Luciferase Assay. Real-time circadian luciferase assays were performed as previously described (Ukai-Tadenuma et al., 2011). Briefly, the day before transfection, NIH3T3 cells or PER2:LUC MEFs were plated onto 35-mm dishes at a density 4×10^5 cells per well. The following day NIH3T3 cells were co-transfected using FuGene6 (Roche) with 1 µg of the indicated luciferase reporter plasmid according to the manufacturer's instructions (n = 3) and cultured at 37 °C. After 72 h, the media in well was

replaced with 2 ml of DMEM containing 10% FBS supplemented with 10 mM HEPES (pH 7.2, ThermoFisher), 0.1 mM luciferin (Promega), antibiotics, and 10 μM forskolin (Fermentek, NIH3T3) or 100 μM dexamethasone (ThermoFisher, PER2::LUC MEFs). Luminescence was measured by a photomultiplier tube (LM2400R, Hamamatsu Photonics) for 1 min at 12 min intervals in a darkroom at 30 °C.

Dual-Luciferase Assay. NIH3T3 cells were plated on 6-well plates at a density of 2×10^5 per well. The following day cells were co-transfected with 0.95 μg of a Firefly *luciferase* reporter plasmid and 50 ng phRL-SV40 plasmid (Renilla luciferase, Promega) as an internal control for transfection efficiency using FuGene6 (Roche). Cells were harvested and assayed by the Dual-Luciferase Reporter Assay System (Promega) according to the manufacturer's instructions 48 h after transfection.

Microscopy and FACS. NIH3T3 cells were plated onto plastic 35-mm dishes or 35-mm imaging dishes (Ibidi) at a density 4×10^5 cells per well. The following day cells were co-transfected using FuGene6 (Roche) with 0.5 μg of the indicated fluorescence reporter plasmids (1 μg total) according to the manufacturer's instructions (n = 3) and cultured at 37 °C. After 72 h, cells were trypsinized and sorted using FACSAria I (BD Biosciences) or analyzed by fluorescence microscopy using a 10× objective (Olympus).

Sleep Phenotyping. Sleep phenotyping was conducted in in 12-week-old (LD) and 14-week-old (DD) mice in a Snappy Sleep Stager (SSS) using *Per2* uORF mutant mice and wild-type littermates as a control (Sunagawa et al., 2016). Briefly, SSS is a non-invasive, respiration-based sleeping staging system in which mice are placed in a chamber connected to a respiration sensor that detects pressure differences between the outside and inside of the chamber. Detailed methods have been described previously (Sunagawa et al., 2016).

Statistical Analyses. Statistical analyses were performed in R version 3.4.3, Prism 7.0, and custom Jupyter notebooks version 6.3. Two-way ANOVA and a Student's t-test was used to test differences in sleep parameters between wild-type and *Per2* uORF mutant mice. For the Student's t-test, data were confirmed gaussian-distributed by a Shapiro-Wilk normality test and an F test was used to check equality of variances. Lomb-Scargle periodograms were implemented using SciPy version 1.7, and cosinor analysis was implemented using

CosinorPy (Moškon, 2020). Statistical significance was defined *P < 0.05, **P < 0.01, ***P < 0.001, and n.s. for not significant.

Sleep and wake parameters. Sleep and wake duration is the mean total sleep and wake duration, respectively, per day over 13 d. P_{sw} is the transition probability from sleep to awake; P_{ws} is the transition probability from awake to sleep. Mathematically, E_i is the i-th epoch, which is either sleep (s) or wake (w). Let N_{XY} ($X,Y \in \{w,s\}$) be the number of elements of the set $\{(E_i, E_{i+1}) \mid E_i = X, E_{i+1} = Y\}$. P_{ws} and P_{sw} are defined as $N_{ws}/(N_{ws} + N_{ww})$ and $N_{sw}/(N_{sw} + N_{ss})$, respectively. The amplitude is defined as the coefficient of variation of sleep time for each 10-min bin over 24 h.

Acknowledgments

We thank Dr. Shihoko Kojima and Dr. Seung-Hee Yoo for PER2::LUC MEFs. We thank Ryohei Narumi for the circadian liver samples and for the use of the mass spectrometry and qPCR data in (Narumi et al., 2016) and Dr. Shigehiro Kuraku for sequencing of the ribosome profiling libraries. We thank all lab members at RIKEN BDR, in particular, Natsumi Hori, Yumika Sugihara for the production of mutant mice, Masako Kunimi, Ruriko Inoue for breeding and helping phenotype measurements of the mutant mice. We thank all lab members at iFReC Systems Immunology lab and iFReC Laboratory for Host Defense, in particular, Kitiya Piboonprai for help with genotyping and Shizuo Akira for his kind support. This work was also supported by grants from Exploratory Research for Advanced Technology (ERATO) grant (JPMJER2001, H.R.U.) from the Japan Science and Technology Agency (JST), KAKENHI Grant-in-Aid from JSPS (Scientific Research S 18H05270, H.R.U.), MEXT Quantum Leap Flagship Program (MEXT QLEAP) Grant Number JPMXS0120330644, AMED under Grant Number JP20am0401011, and the intramural Grant-in-Aid from the RIKEN Center for Biosystems Dynamics Research to H.R.U. This work was supported by the Human Frontiers Science Program and a JSPS Grant-in-Aid for Early Career Scientists (18K14755 to AM).

List of Figures and Tables

Figure 1 | Measuring translation and protein from same liver samples for 16 circadian mRNAs

Figure 2 | Upstream open reading frames (uORFs) diminish protein expression

Figure 3 | The Per2 uORF is evolutionarily conserved and suppresses PER2 expression.

Figure 4 | Disruption of the *Per2* uORF reduces sleep in mice.

Supplementary Figure 1 | Analyzing mRNA expression, translation activity, and absolute protein copy number levels in the same mice liver samples over the course of a day (related to Figure 1).

Supplementary Figure 2 | Construction of ribosome profiling cDNA libraries (related to Figure 1).

Supplementary Figure 3 | Phase analysis (related to Figure 1).

Supplementary Figure 4 | RNA, ribosome profiling, and protein phase comparison to LD conditions from previous studies (Atger et al., 2015; Janich et al., 2015; Wang et al., 2017) (related to Figure 1).

Supplementary Figure 5 | Measuring translation and RNA expression from same liver samples for 16 circadian mRNAs (related to Figure 1).

Supplementary Figure 6 | Distribution of upstream open reading frames in clock transcripts (related to Figure 2).

Supplementary Figure 7 | Detailed analysis of the Per2 uORF (related to Figure 3).

Supplementary Figure 8 | Disruption of the *Per2* uORF in mice (related to Figure 4).

Supplementary Figure 9 | Detailed analysis of 12 h light:12 h dark (LD) sleep parameters (related to Figure 4).

Supplementary Figure 10 | Cosinor analysis of LD and constant darkness (DD) circadian rhythm parameters (related to Figure 4).

Supplementary Table 1 | Sequence statistics for ribosome profiling data showing the number of reads per sample, number of reads mapped to rRNA, unmapped reads, and mapped reads. Library concentrations were analyzed by bioanalyzer, and index primer sequences are shown.

Supplementary Table 2 | JTK analysis of ribosome profiling data for circadian (BH.Q < 0.05) transcripts.

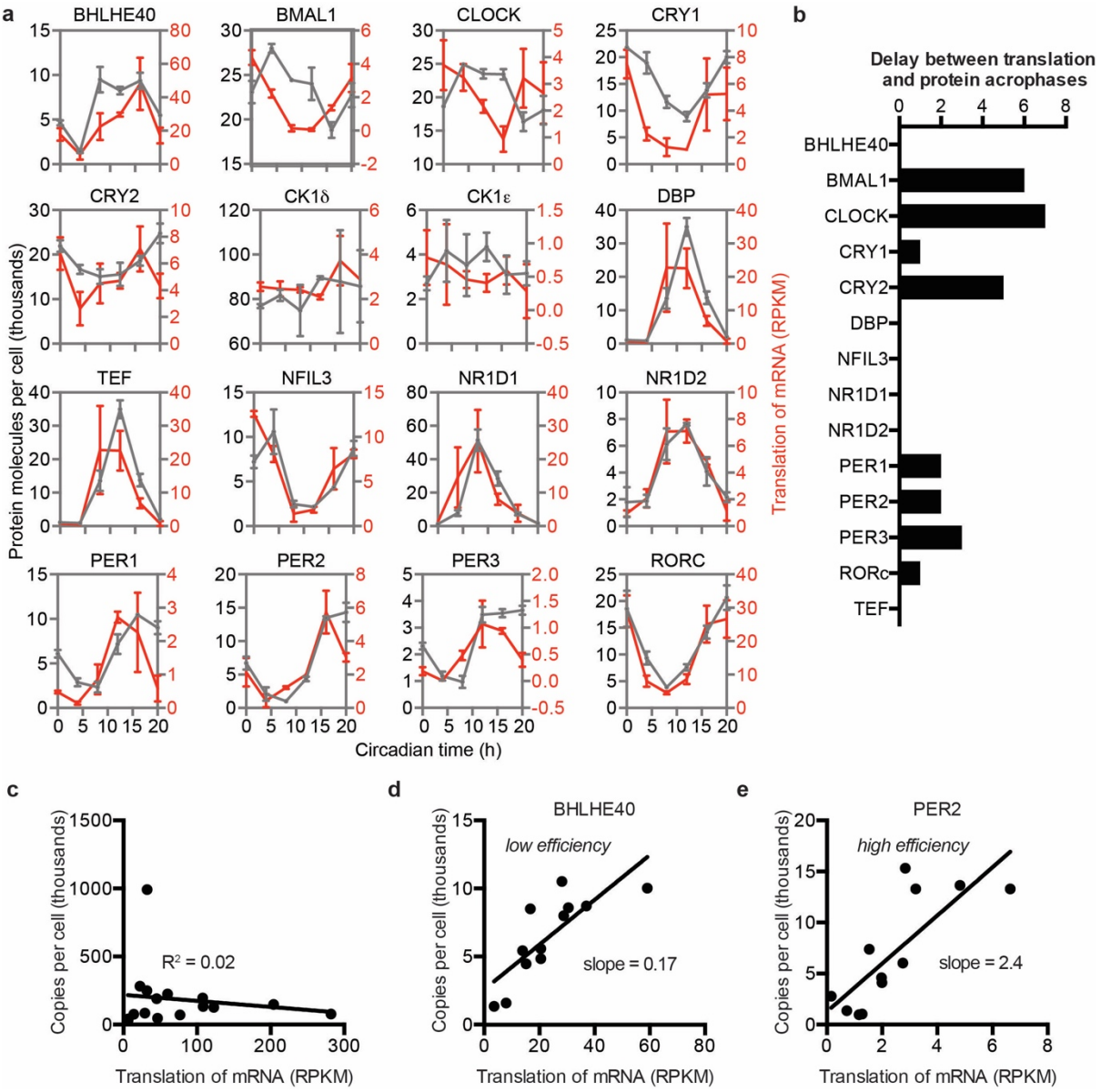

Figure 1 | Measuring translation and protein from same liver samples for 16 circadian mRNAs. a Time course of the quantified proteins and the corresponding translation level. Protein concentration (gray) is expression as copies per cell assuming the total amount of protein per cell is 0.5 ng. Protein concentration is the average for all quantified peptides for a given protein. Translation level (red) is expressed as reads per kilobase of transcript per million mapped reads (RPKM). Error bars are standard deviation of the two replicates. Data from protein copy numbers are derived from (Narumi et al., 2016). **b** Phase delay between translation and protein level. Copies per cell were averaged from all peptides for each protein. JTK analysis was used to estimate the phases for these averaged protein levels and for translation RPKM levels. **c** Linear regression analysis comparing translation levels to protein copies per cell averaged over 24 hours shows that there is no correlation between translation level and protein abundance **d, e** Linear regression analysis comparing translation

levels to protein copies per cell at each sampled time point shows that some mRNAs like Bhlhe40 (**d**) are translated into protein with low efficiency whereas other mRNAs like Per2 (**e**) and translated into protein with high efficiency.

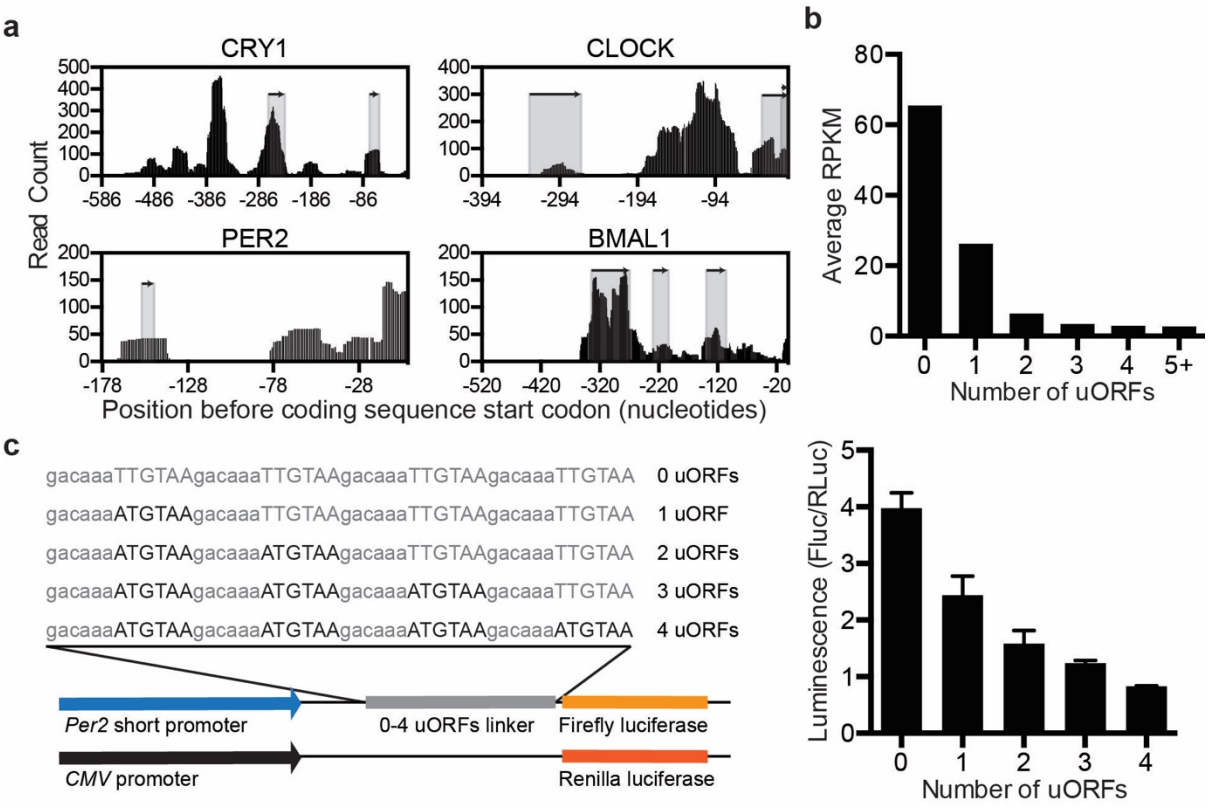

Figure 2 | Upstream open reading frames (uORFs) suppress protein expression. a The 5' UTRs of *Cry1*, *Clock*, *Per2*, and *Bmal1* transcripts contain at least one uORF (shaded regions). Distribution of raw read counts from ribosome profiling data (black bars) show ribosomes bounds in regions corresponding to uORFs. **b** Global distribution of uORFs compared to ribosome profiling translation level (RPKM) shows that mRNAs with more uORFs are translated less compared to mRNAs with fewer uORFs. **c** Introduction of a variable number of synthetic uORFs represses relative luminescence from a *Per2* short promoter in a dose-dependent manner.

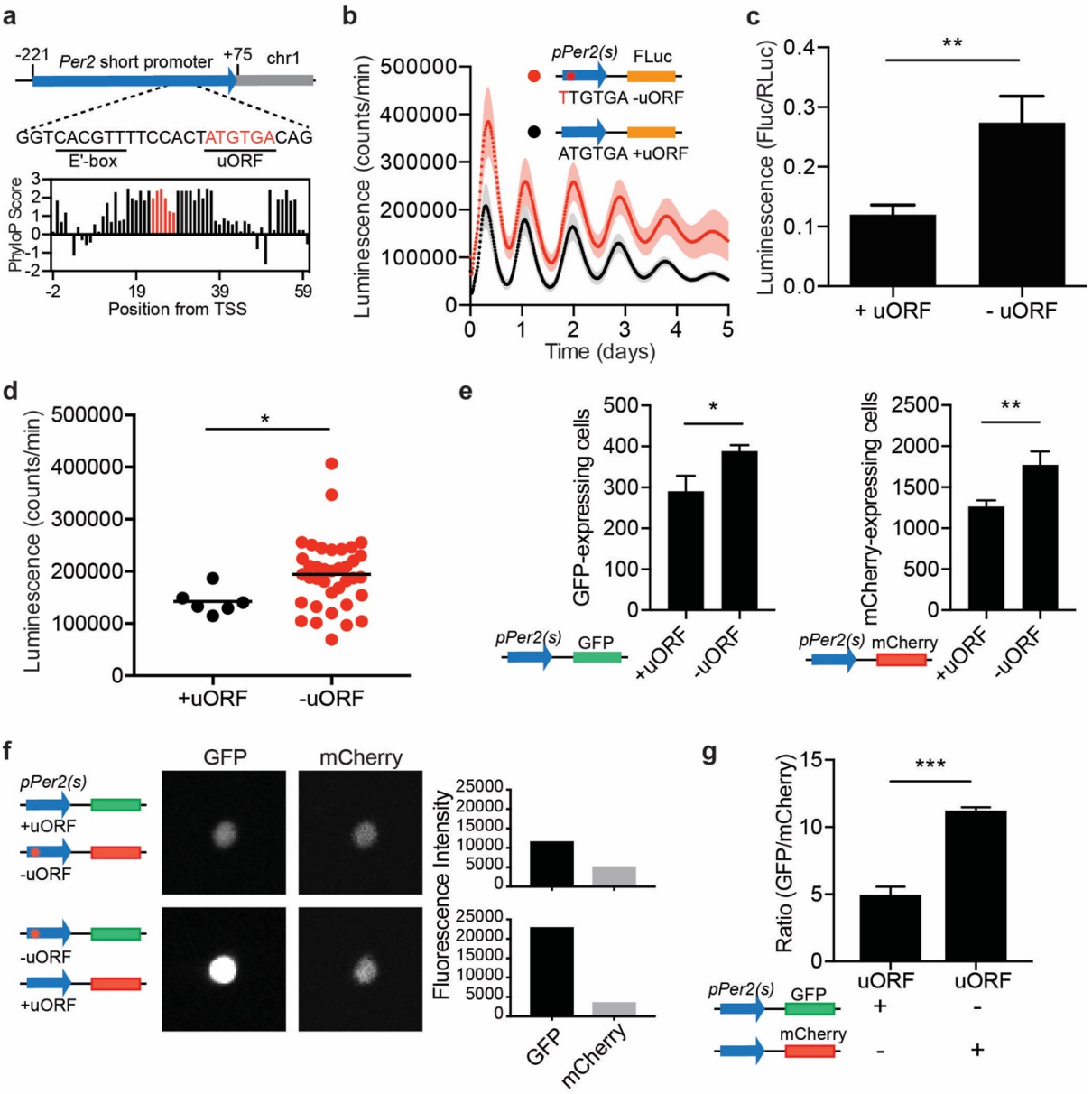

Figure 3 | The Per2 uORF is evolutionarily conserved and suppresses PER2 expression. **a** Genomic position of the Per2 short promoter, which contains an E' box and uORF. Evolutionary conservation scores according to UCSC genome browser among 22 mammalian species (black bars). Evolutionary conservation of the uORF (red bars). **b** Mutation of the Per2 uORF (ATGTGA to TTGTGA) increases the luminescence expression level of the reporter as measured by bioluminescent recording. Reporter containing uORF (black), reporter lacking uORF (red). Shaded region is SD. **c** Relative luminescence experiments of plasmids in (**b**). **d** Average bioluminescence expression between 24 h and 72 h after dexamethasone stimulation of PER2:LUC MEFs and PER2:LUC MEFs where the Per2 uORF has been mutated by CRISPR/Cas9-mediated homologous recombination. **e** 3T3 cells were transfected with pPer2 expressing GFP or mCherry with or without a mutation in the

Per2 uORF. After three days, 10,000 cells were analyzed by FACS and the number of green or red cells in the population is shown. **f** Representative example of individual cells from (**e**) imaged by microscopy (left) and quantified (right). **g** Microscopy analysis of GFP/mCherry ratios of cells (n >10) from (**e**).

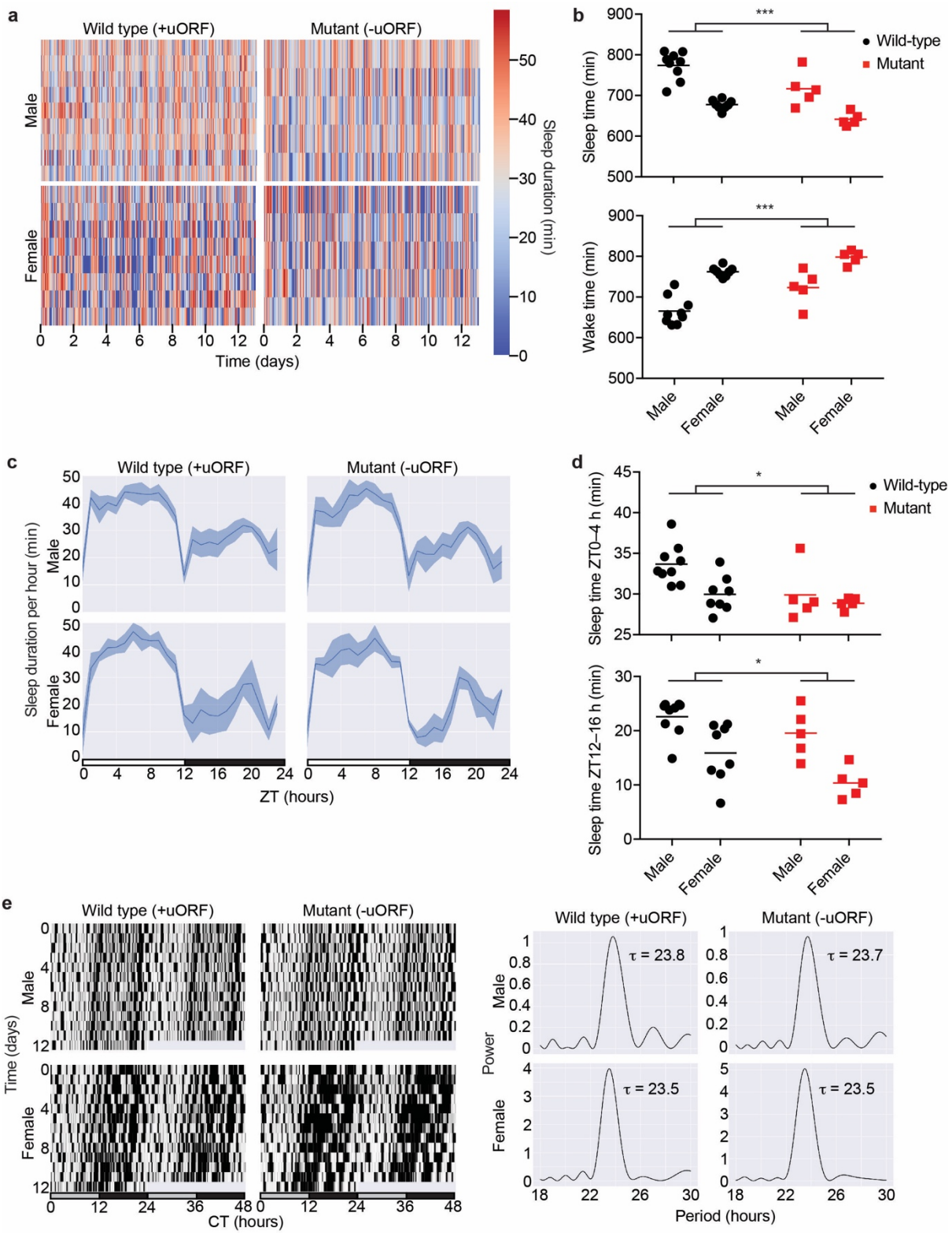

Figure 4 | Disruption of the *Per2* uORF reduces sleep in mice. a Sleep duration per hour over 13 d in 12-h light/12-h dark (LD) conditions for *Per2* uORF mutant and wild-type male and female mice. Each row indicates data from one mice. **b** Mean sleep (*top*) and wake (*bottom*) duration over 24 h, averaged over 13 d. Red, *Per2* uORF mutant mice. Black, wild-type. **c** Sleep duration per hour over 24 h, averaged over 13 d for *Per2* uORF mutant and

wild-type male and female mice. Blue lines indicate mean sleep duration at each time of day for each strain. Shaded area, SD for each time point. **d** Mean sleep duration per hour averaged over 13 d during the early morning (*top*) and early evening (*bottom*). Red (Per2 uORF mutant) and black (wild-type) dots are individual mice; lines indicate mean (**c, d**). (*P < 0.05, **P < 0.01, ***P < 0.001; SI Appendix, SI Materials and Methods). **e** Representative double-plotted actograms of sleep duration per 6 min bins of wild-type and *Per2* uORF mutant mice in constant darkness (DD) over 12 d (*left*) and corresponding periodograms (*right*).

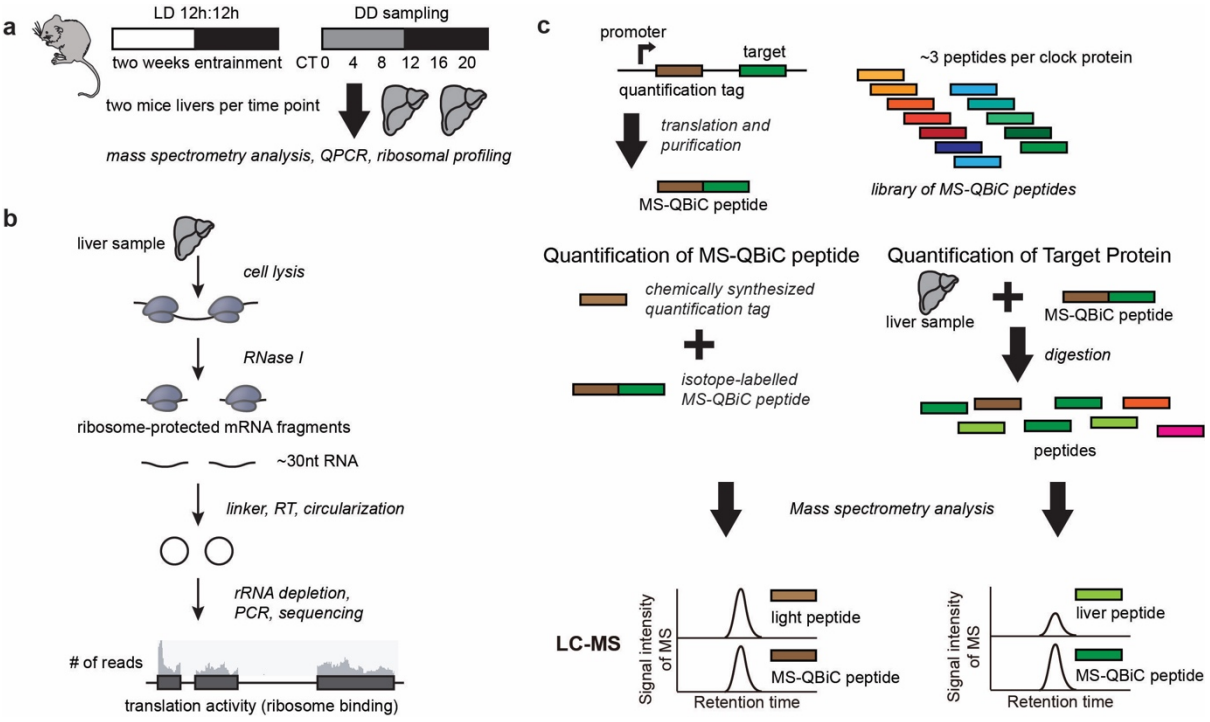

Supplementary Figure 1 | Analyzing mRNA expression, translation activity, and absolute protein copy number levels in the same mice liver samples over the course of a day (related to Figure 1). a All mice were carefully kept and handled according to the RIKEN Regulations for Animal Experiments. Eight to ten-week-old-male mice (C57BL/6N, Japan SLC) were entrained under a 12–12 h light-dark condition (400 lux) for 2 weeks. After transferring to constant darkness, mice were sacrificed every 4 h over 1 day (i.e. CT0, 4, 8, 12, 16, and 20) for proteomic and translation analyses or every 4 h over 2 days (i.e. CT0, 4, 8, 12, 16, 20, 24, 28, 32, 36, 40, and 44) for qPCR analyses. **b** Two mice livers at seven different circadian time points were lysed and ribosomes were isolated by a sucrose cushion. Ribosome-protected mRNA fragments were extracted, reverse transcribed, and circularized into a library. Libraries were depleted of the common most abundant rRNA, PCR amplified and sequenced (~1.02 billion reads). **c** Schematic description of the MS-QBiC workflow. A purification-tag, a quantification-tag, and a tryptic peptide of the target protein (target peptide) were sequentially arrayed as a single peptide sequence (MS-QBiC peptide). The target peptide sequence was attached by one- or two-step PCR. The MS-QBiC peptide was synthesized in the PURE system in the presence of stable isotope-labeled Arg and Lys for isotopic labeling both the quantification-tag and the target peptide. Trypsin digestion of purified MS-QBiC peptide produced equal amounts of isotopically labeled quantification-tag and target peptide. The quantification-tag was used to measure purified MS-QBiC peptide and the target peptide was used as an internal standard for target protein quantification.

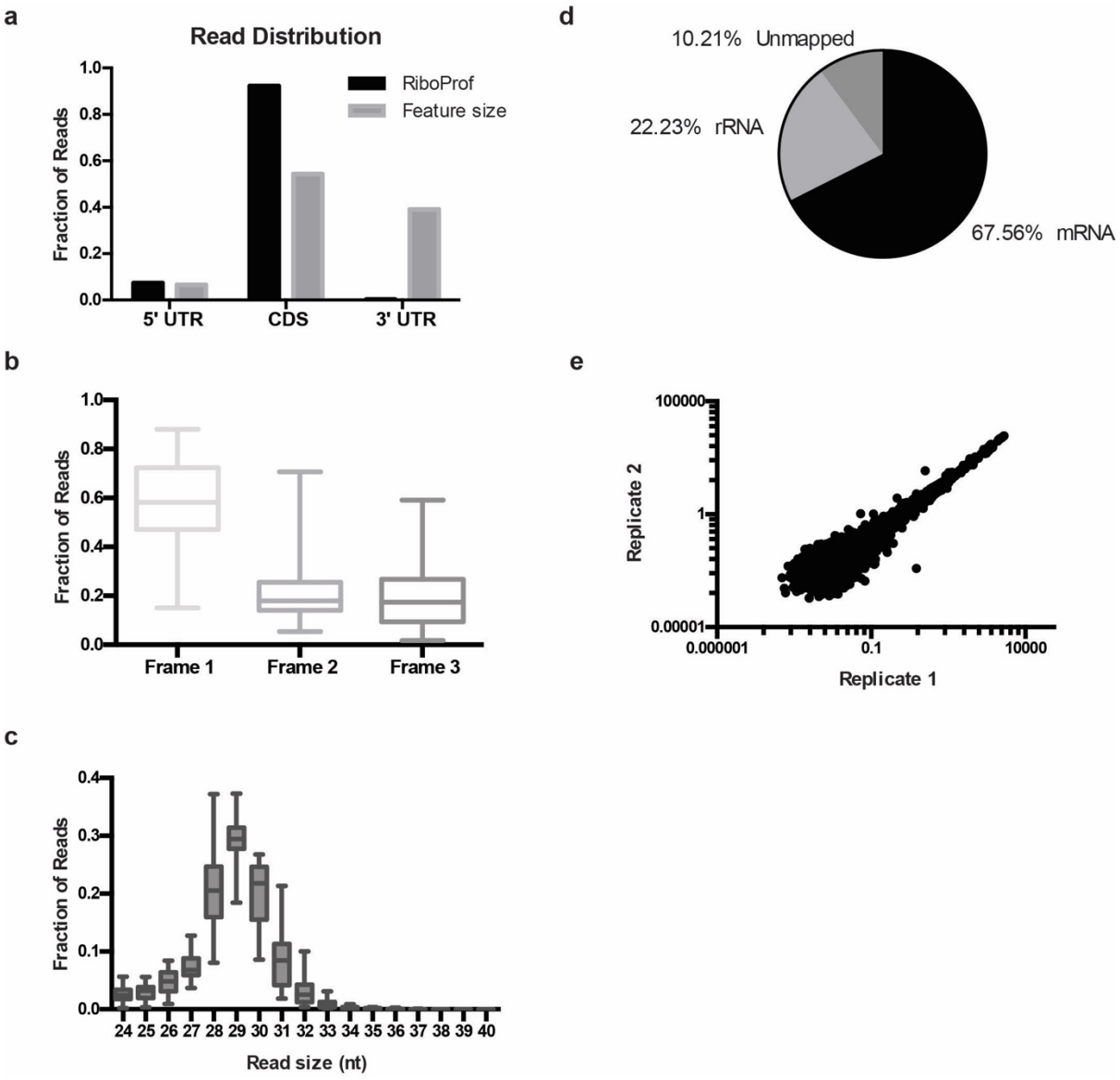

Supplementary Figure 2 | Validation of ribosome profiling cDNA libraries (related to Figure 1). a Read distribution within 5'UTRs, CDS, and 3'UTRs compared with the size of those features. Ribosome profiling reads are enriched for the CDS and 5'UTR, and relatively few reads map to the 3'UTR. **b** Frame analysis of ribosome profiling reads of single protein isoform mRNAs shows a preference for frame 1 (the coding frame). Box-and-whisker plots: midline, median; box, 25th and 75th percentiles. Whiskers are minimum and maximum values. **c** Box and whisker plots show the distribution of read lengths from all sequences. The majority of reads were between 27 and 32 nt, which matches the footprint size of the ribosome. **d** Summary of mapped reads. **e** Correlation of RPKM between replicate 1 and replicate 2 at CT00 shows a high degree of correlation between the translation level of individual mRNAs.

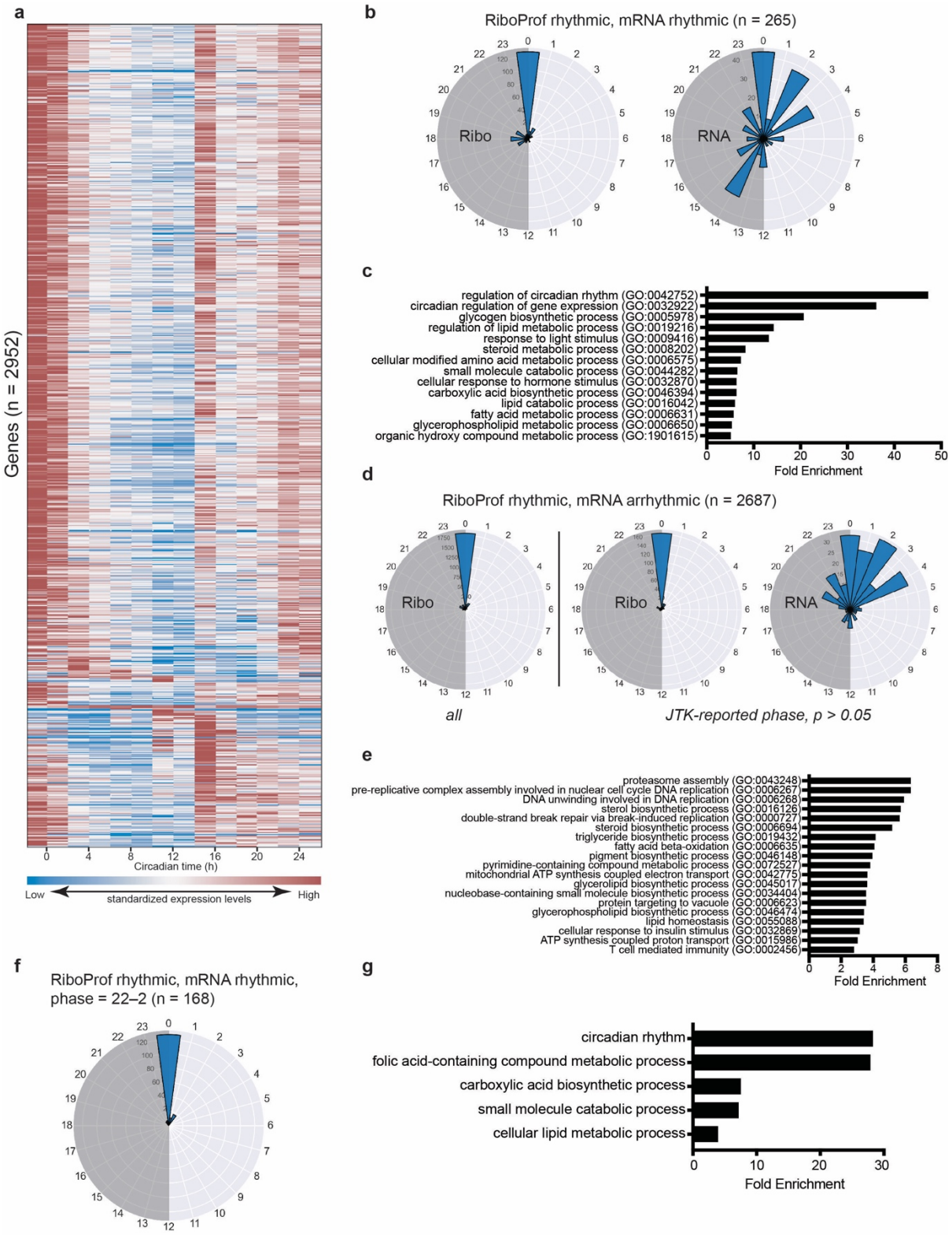

Supplementary Figure 3 | Phase analysis (related to Figure 3). a Heat map of ribosome profiling rhythmic transcripts identified by JTK cycling analysis ($P < 0.05$) showing RPKM data over 24 hours for 2952 genes. Transcripts are sorted by phase, and RPKM values are normalized within each gene (row). Note that most transcripts peak at CT00 (red bars in first two columns). **b** Polar histogram showing the ribosome profiling (*left*) and RNA (*right*)

phase distribution of the 265 ribosome profiling rhythmic and mRNA rhythmic transcripts. **c** Panther analysis of gene ontology biological processes based on genes in (**b**) showing an increase in circadian rhythm regulation pathways and metabolic processes. **d** Polar histogram showing the ribosome profiling phase distribution (*left*) of the 2687 ribosome profiling rhythmic transcripts that did not reach significance in mRNA rhythmicity. Ribosome profiling (*middle*) and RNA (*right*) polar histograms for transcripts with an mRNA JTK-reported phase $P > 0.05$ are also shown. **e** Panther analysis of gene ontology biological processes based on the 2687 genes in (**d**). **f, g** There were 168 transcripts from (**b**) with a phase distribution between CT22-CT00 (**f**) corresponding to circadian rhythm and metabolism processes by Panther analysis (**g**). Note that this group includes NR1D1-regulated transcripts including *Npas2*, *Arntl*, *Cry1*, *Nfil3*, and *Clock*.

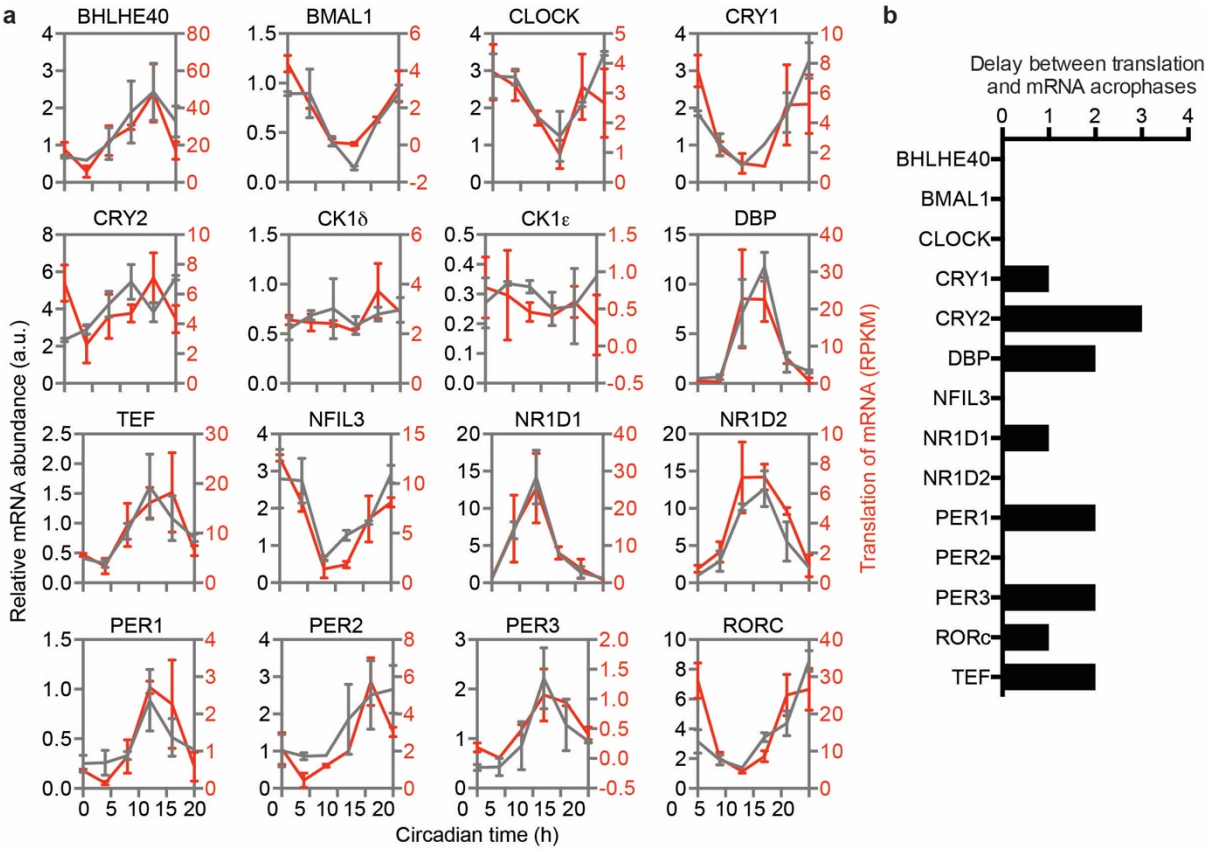

Supplementary Figure 4 | Measuring translation and RNA expression from the same liver samples for 16 circadian mRNAs (related to Figure 1). a Time course of the quantified RNA expression levels by qPCR and the corresponding translation level. RNA levels (grey) were derived from data in Narumi et al., 2016. Translation level (red) is expressed as reads per kilobase of transcript per million mapped reads (RPKM). Error bars are the standard deviation of the two replicates. **b** Phase delay between mRNA expression and translation. Expression levels of each mRNA were quantified by qPCR. Absolute cDNA abundance was calculated using the standard curve obtained from mouse genomic DNAs, and JTK analysis was used to estimate the phase of each mRNA.

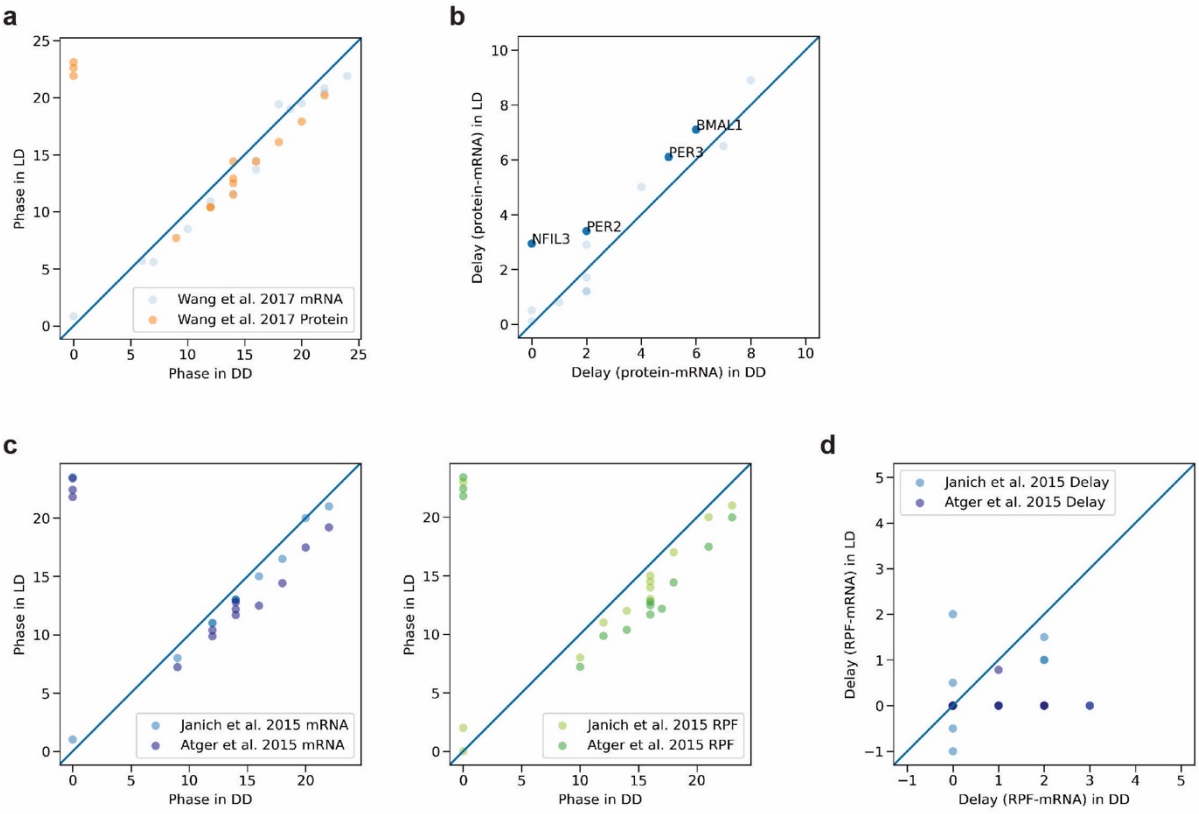

Supplementary Figure 5 | Comparison of RNA expression, translation, and protein production phases in DD (this study) to previously published studies in LD conditions (Atger et al., 2015; Janich et al., 2015; Wang et al., 2017). a Protein (orange) and mRNA (blue) phases for 16 selected circadian genes observed in DD (this study) or LD (Wang et al., 2017). **b** The delay between mRNA and protein phases observed in DD (this study) or LD (Wang et al., 2017). Several proteins (labeled) including PER2 had a greater than one hour difference in protein-mRNA delay between LD and DD conditions. **c** The mRNA (*left*) and ribosome profiling (*right*) phases for 16 selected circadian genes observed in DD (this study) or LD (Janich et al., 2015) and (Atger et al., 2015). **d** The delay between mRNA and ribosome profiling phases observed in DD (this study) or LD (Janich et al., 2015) and (Atger et al., 2015).

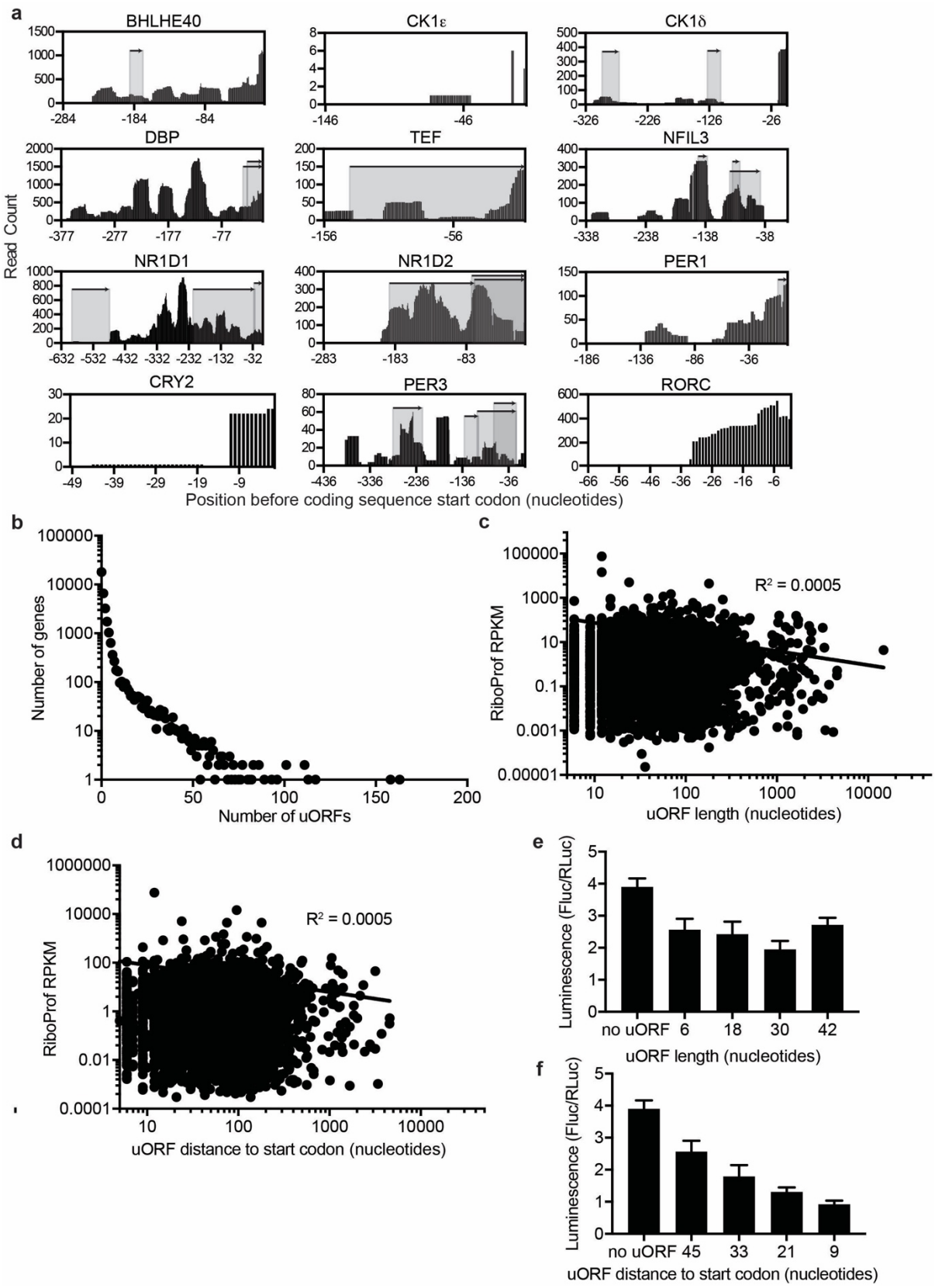

Supplementary Figure 6 | Distribution of upstream open reading frames in clock transcripts (related to Figure 2). a The 5' UTRs of *Bhlhe40*, *Ck1e*, *Ck1d*, *Dbp*, *Tef*, *Nfil3*, *Nr1d1*, *Nr1d2*, *Per1*, *Cry2*, *Per3*, and *Rorc* transcripts, location of uORFs (shaded regions),

and raw read counts from the ribosome profiling data (black bars). **b** The number of transcripts with a given number of uORFs. **c** The relationship between the length of an uORF and ribosome binding in the corresponding ORF. **d** The relationship between the distance of an uORF to the ORF start codon and ribosome binding in the corresponding ORF. **e** Introduction of a single uORF in the *Per2* short promoter of different lengths does not alter the relative luminescence of the *Per2* luciferase reporter. **f** The distance of a single uORF in the *Per2* short promoter to the start codon correlates with the relative luminescence of the *Per2* luciferase reporter.

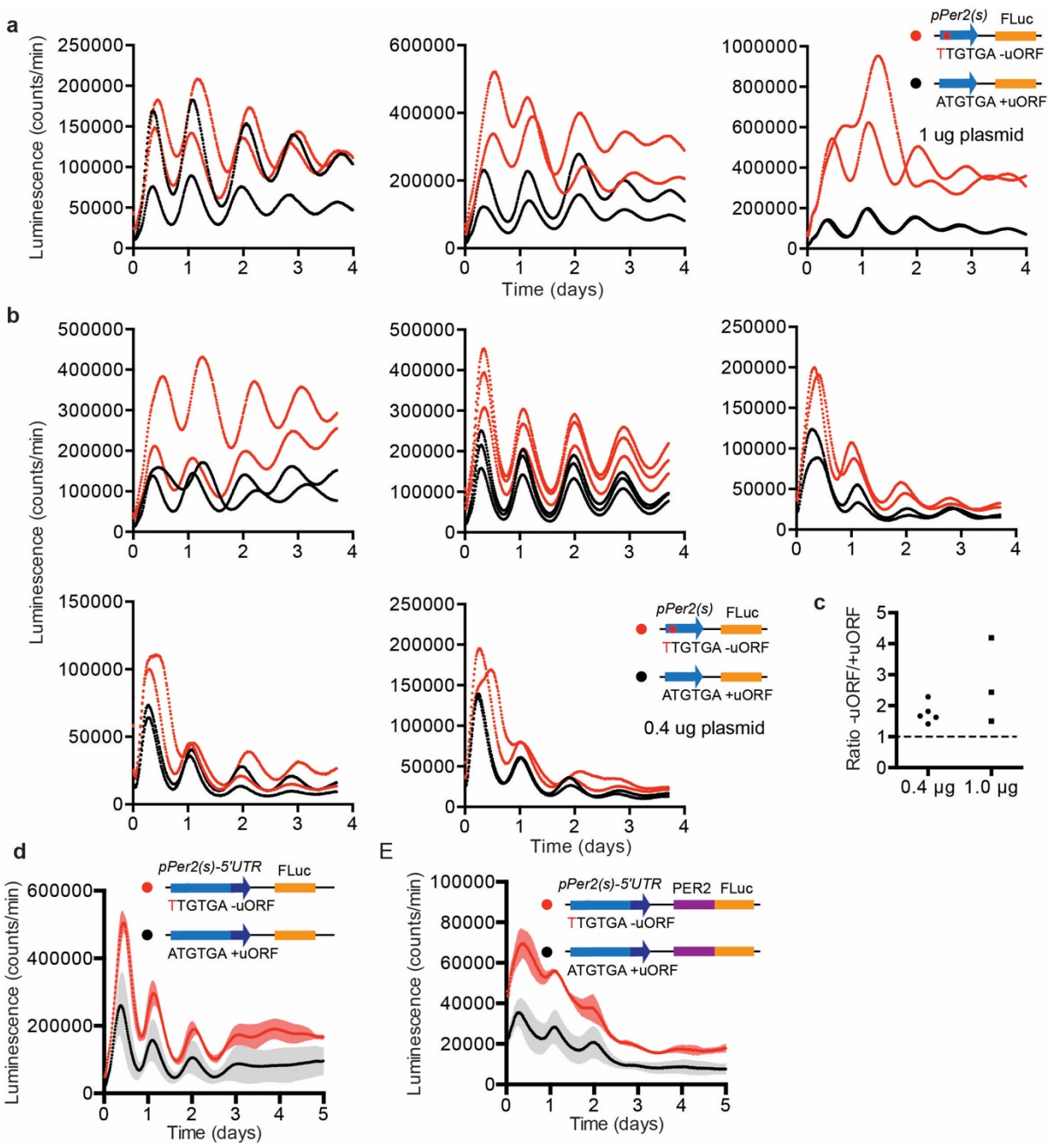

Supplementary Figure 7 | Detailed analysis of the *Per2* uORF (related to Figure 3). a Bioluminescent recording of 3T3 cells transfected with the *Per2* short promoter containing (black) and lacking (red) the *Per2* uORF at 1 ug (**a**) and 0.4 ug (**b**) transfected plasmid. Each graph is an independent experiment performed on a different day, multiple traces on the same graph indicate different transfected plates. Data from the upper middle panel of (**b**) was used to produce Figure 3B. **c** The -uORF luminescence levels in experiments (**a**) and (**b**) were normalized by the corresponding +uORF luminescence levels for each experiment. Ratios above 1 indicate a higher level of reporter expression in -uORF-expressing cells (n = 5 independent experiments with at least 2 transfected plates per experiment for 0.4 µg transfected plasmid, and n = 3 for 1.0 µg transfected plasmid). **d** Mutation of the *Per2* uORF

(ATGTGA to TTGTGA) with the full-length *Per2* 5' UTR (red) increases the luminescence expression level of the reporter as measured by bioluminescent recording compared to that of a reporter containing the uORF (black). Shaded region is SD. **e** (top) Mutation of the *Per2* uORF (ATGTGA to TTGTGA) with the full-length *Per2* 5' UTR and PER2 protein (red) increases the luminescence expression level of the reporter as measured by bioluminescent recording compared to that of a reporter containing the uORF (black). Shaded region is SD.

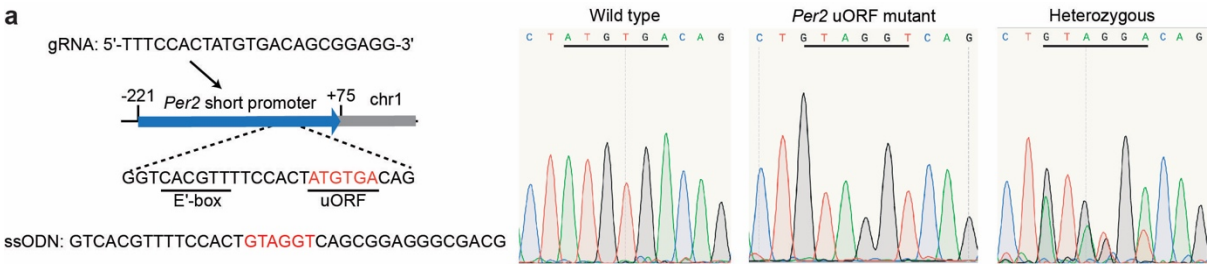

Supplementary Figure 8 | Disruption of the *Per2* uORF in mice (related to Figure 4). a An ssODN replaced the *Per2* uORF (AUGUGA) with a mutant version (GUAGGU) in which both the start and stop codons were mutated. The diagram shows the location of the CRISPR gRNA and upstream E' box within the *Per2* promoter region. b. Representative Sanger sequencing results from wild-type, *Per2* uORF mutant, and heterozygous mice are shown.

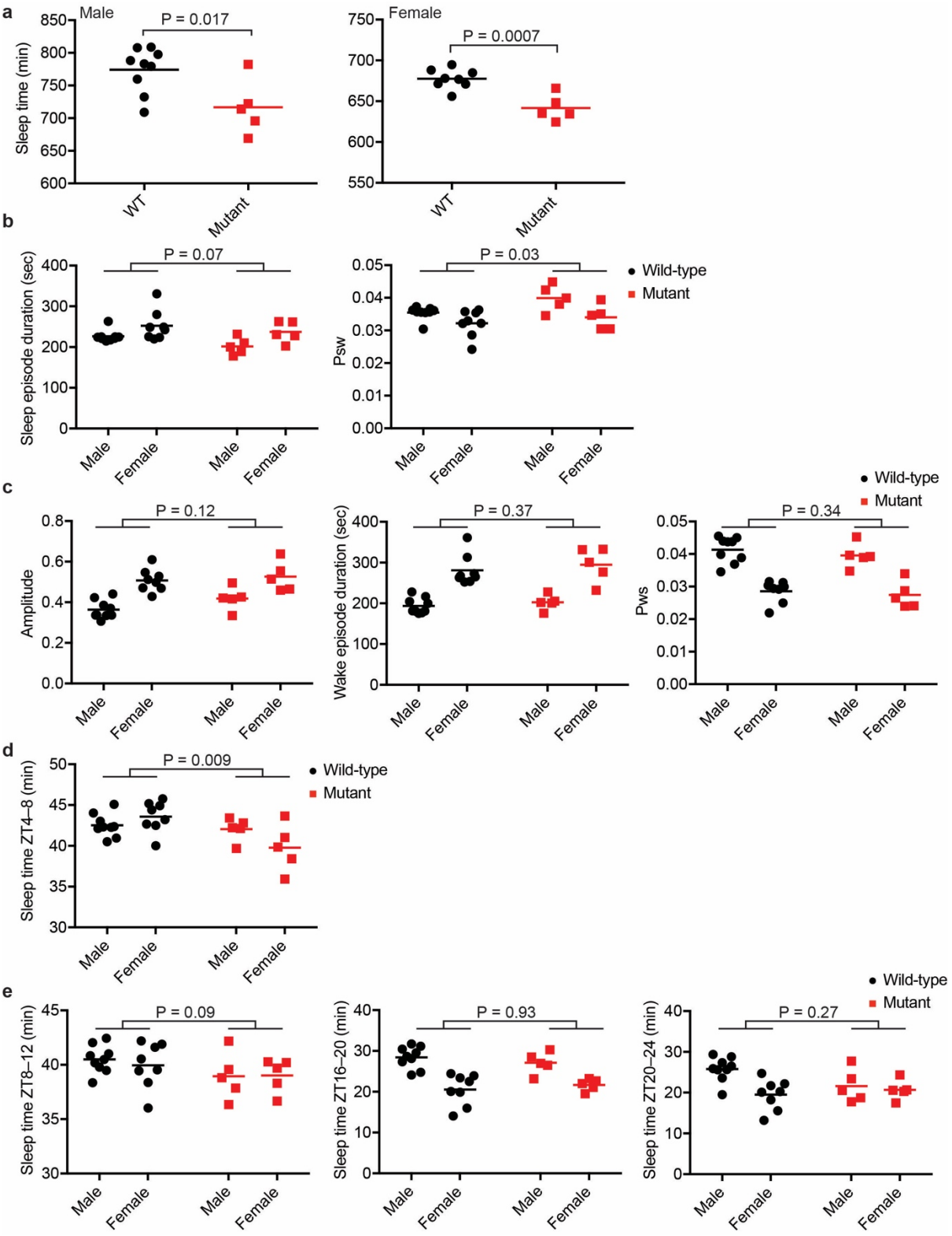

Supplementary Figure 9 | Detailed analysis of 12 h light:12 h dark (LD) sleep parameters (related to Figure 4). a Mean sleep duration over 24 h averaged over 13 d for male (*left*) and female (*right*) mice. Red, *Per2* uORF mutant mice. Black, wild-type. P values, Student's unpaired t-test. **b** Sleep episode duration (*left*) was shorter and P_{sw} was higher (*right*) in *Per2* uORF mutant mice than in wild-type mice, but the differences were not

significant. **c** There was no significant differences in amplitude (*left*), wake episode duration (*middle*), and P_{ws} (*right*) between *Per2* uORF mutant and wild-type mice. **d, e** Mean sleep duration per hour averaged over 13 d for 4-h windows from ZT4–8 (**d**) and ZT8–12, ZT16–20, and ZT20–24 (**e**). Detailed descriptions of the sleep parameters are described in SI Appendix, SI Materials and Methods.

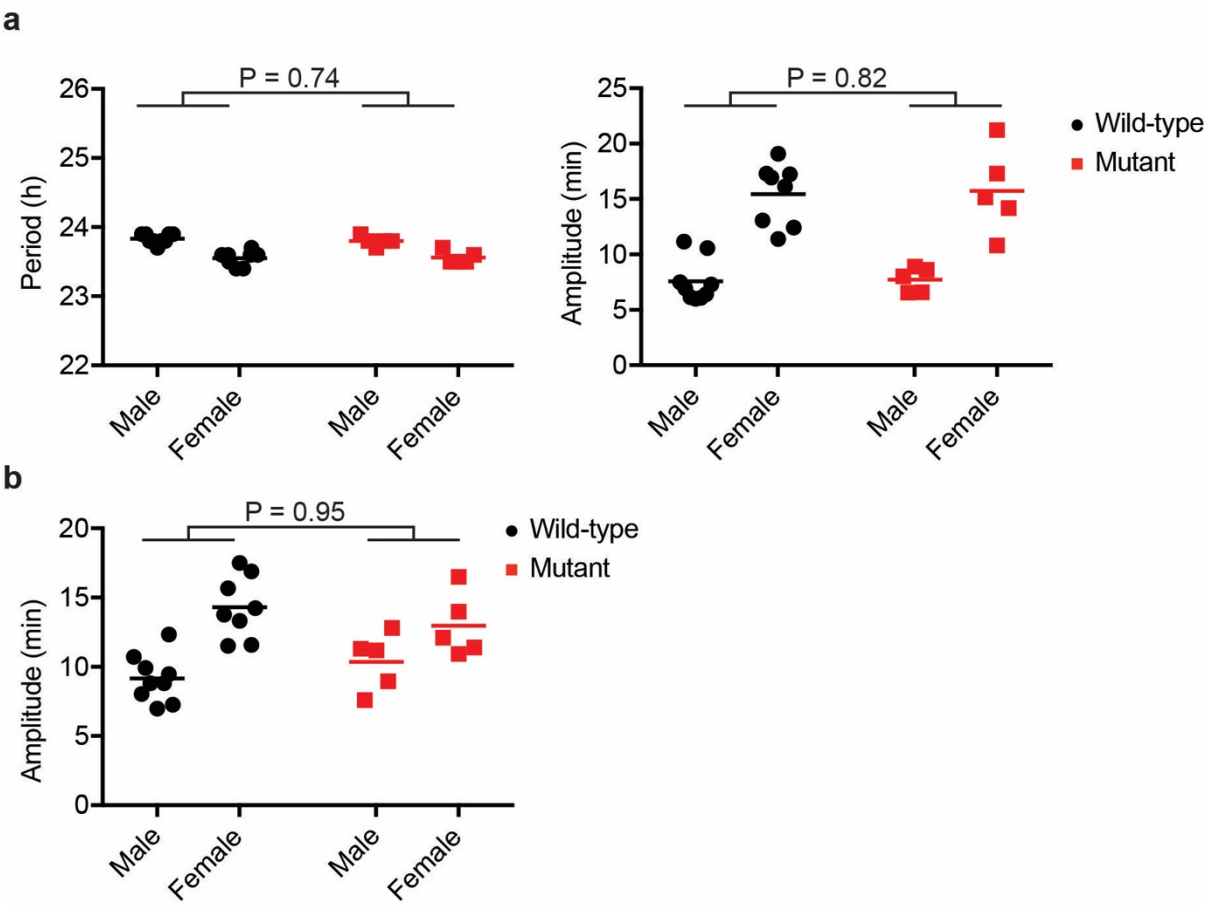

Supplementary Figure 10 | Cosinor analysis of LD and DD circadian rhythm parameters (related to Figure 4). a Cosinor analysis of the period (*left*) and amplitude (*right*) of wild-type and *Per2* uORF mutant mice in constant darkness (DD) conditions. **b** Cosinor analysis of the amplitude of wild-type and *Per2* uORF mutant mice in LD conditions.

Sample	CT	Reads	rRNA aligned	rRNA (%)	Unmapped	Unmapped (%)	Mapped	Mapped (%)
A1	0	67420894	31637068	47	6493665	10	29290161	43
A2	4	79568956	40132748	50	6120169	8	33316039	42
A3	8	92923717	46040656	50	7305061	8	39578000	43
A4	12	89178791	37939665	43	4558237	5	46680889	52
A5	16	73866781	37993296	51	3002837	4	32870648	44
A6	20	57310601	29343482	51	3785209	7	24181910	42
A7	24	57919810	30413247	53	1903635	3	25602928	44
B1	0	82543812	46972438	57	5223484	6	30347890	37
B2	4	76767842	45784936	60	2978293	4	28004613	36
B3	8	67206206	31921429	47	2040538	3	33244239	49
B4	12	77788251	44039811	57	2632701	3	31115739	40
B5	16	73477498	42486921	58	2420565	3	28570012	39
B6	20	79546292	41792698	53	4794899	6	32958695	41
B7	24	91267817	37921444	42	20546228	23	32800145	36
Total		1066787268	544419839	51	73805521	7	448561908	42

1

2

3 **Supplementary Table 1 | Sequence statistics for ribosome profiling data showing the**
4 **circadian time (CT), number of reads per sample, number of reads mapped to rRNA,**
5 **unmapped reads, and mapped reads.**

6

Name	RefSeq ID	BH.Q	ADJ.P	PER	LAG	AMP	CT00A	CT00B	CT04A	CT04B	CT08A	CT08B	CT12A	CT12B	CT16A	CT16B	CT20A	CT20B	CT24A	CT24B
Sigmar1	NM_001286541	0.00	1.23E-07	24	0	8.1	36.2	32.8	15.6	16.6	8.7	9.2	3.7	7.3	13.5	9.7	20.2	22.8	30.2	21.9
Tardbp	NM_145556	0.01	5.99E-07	24	0	1.2	4.9	4.2	2.3	1.7	1.1	1.0	0.3	1.0	1.9	2.0	2.4	2.7	3.9	3.1
Aqp8	NM_001109045	0.01	2.20E-06	24	0	6.5	26.2	22.8	12.4	7.4	3.4	3.1	1.0	1.4	4.3	2.3	14.2	11.4	17.9	17.4
Rdh11	NM_021557	0.01	2.20E-06	24	0	5.6	27.3	21.1	12.2	9.5	7.5	9.4	4.1	3.3	9.5	7.6	14.7	20.0	19.6	16.1
Arntl	NM_001243048	0.01	2.20E-06	24	0	2.2	4.7	4.1	2.0	2.4	0.0	0.3	0.0	0.1	1.5	1.3	2.6	3.8	3.7	3.0
Ncald	NM_001170866	0.01	2.20E-06	24	4	1.7	5.0	4.6	5.7	5.5	3.5	3.4	2.1	1.1	2.4	2.0	3.3	3.4	5.1	5.1
Ppard	NM_011145	0.01	2.20E-06	24	0	1.0	5.9	4.9	0.5	1.4	0.3	0.3	0.0	0.1	1.1	0.6	2.8	2.1	5.5	3.1
Rnf144a	NM_001081977	0.01	2.20E-06	24	0	0.6	2.9	4.1	1.3	1.3	0.6	0.5	0.0	0.2	1.0	0.7	1.9	1.0	1.7	1.9
Dennd2d	NM_001093754	0.01	2.20E-06	24	0	0.3	1.7	1.4	0.9	0.9	0.8	0.6	0.4	0.4	1.0	0.9	1.3	1.0	1.3	1.5
Pnrc1	NM_001033225	0.01	6.89E-06	24	0	25.7	59.5	68.6	43.2	40.4	16.3	11.6	11.1	8.5	34.7	16.5	34.4	44.1	44.1	49.7
Aqp8	NM_007474	0.01	6.89E-06	24	0	21.1	98.7	86.8	55.5	31.4	17.2	12.9	7.7	6.3	19.0	15.4	37.2	49.7	61.4	51.7
Pgd	NM_001081274	0.01	6.89E-06	24	0	5.6	21.4	22.5	14.4	8.9	8.5	9.1	7.1	6.7	11.9	13.7	15.2	17.2	18.2	16.0
Cks2	NM_025415	0.01	6.89E-06	24	0	3.4	28.2	22.4	13.1	11.4	6.1	8.6	2.4	6.7	10.1	9.6	12.4	10.5	16.3	13.9
Capn2	NM_009794	0.01	6.89E-06	24	0	2.0	11.3	12.4	7.7	6.4	4.6	4.8	4.3	3.0	6.1	6.6	6.5	7.4	9.4	7.9
Tjp2	NM_001198985	0.01	6.89E-06	24	0	1.2	5.2	4.0	3.3	2.4	1.6	1.9	1.6	1.0	3.1	2.2	2.6	3.5	3.7	3.3
Wee1	NM_009516	0.01	6.89E-06	24	16	1.1	0.6	0.6	0.1	0.3	2.0	1.0	2.3	2.1	3.8	2.9	1.2	1.3	0.7	0.4
Clpx	NM_001044389	0.02	1.89E-05	24	0	26.1	67.5	67.5	57.7	48.2	18.4	16.1	9.1	5.6	22.4	17.0	29.7	46.0	58.6	63.6
Nampt	NM_021524	0.02	1.89E-05	24	18	11.4	14.6	13.2	6.6	6.9	7.4	9.3	31.1	22.1	43.9	32.4	18.2	20.5	13.3	10.9
Pmvk	NM_026784	0.02	1.89E-05	24	0	6.8	40.6	32.2	9.7	7.2	4.6	5.3	4.2	4.3	8.9	9.5	18.5	24.3	23.0	16.8
Nat8	NM_023455	0.02	1.89E-05	24	22	4.2	7.1	9.3	5.8	4.3	2.7	3.3	3.3	3.1	8.4	7.6	10.2	9.8	8.8	8.5
Evi5	NM_007964	0.02	1.89E-05	24	0	2.5	11.3	13.3	9.8	8.5	5.6	5.5	5.1	2.6	7.9	6.0	6.7	8.9	9.1	9.9
Dpp9	NM_172624	0.02	1.89E-05	24	0	2.0	12.0	10.9	7.5	6.9	4.7	4.0	2.4	3.4	5.9	4.9	6.2	6.6	10.5	7.1
Tjp3	NM_001282095	0.02	1.89E-05	24	0	1.8	5.5	5.4	3.8	2.0	1.0	1.3	0.7	0.6	3.5	1.8	3.2	3.2	4.4	4.0
Bloc1s5	NM_139063	0.02	1.89E-05	24	0	1.6	13.6	11.4	8.2	7.8	6.6	5.5	4.0	5.5	7.8	6.5	7.0	8.8	10.0	8.6
Gpcpd1	NM_001042672	0.02	1.89E-05	24	12	1.5	3.0	2.4	3.8	3.2	9.1	4.8	23.0	11.7	4.5	4.3	3.0	2.9	2.1	1.9
Dock6	NM_177030	0.02	1.89E-05	24	0	0.8	3.2	2.7	1.9	1.2	0.8	0.8	0.5	0.4	1.4	1.4	1.6	2.0	2.3	1.7
Fam222a	NM_001004180	0.02	1.89E-05	24	0	0.5	2.4	3.4	0.4	1.1	0.7	0.4	0.0	0.2	0.9	0.7	1.2	1.4	2.2	1.2
Elovl3	NM_007703	0.03	4.69E-05	24	1	182.4	634.0	590.9	326.6	365.0	49.3	64.1	27.1	24.1	99.2	40.9	209.9	318.8	529.0	450.4
Hacl1	NM_019975	0.03	4.69E-05	24	0	77.4	247.4	188.7	134.6	114.1	75.0	64.3	46.6	42.3	140.7	84.9	147.7	199.3	194.5	180.9
Cyp8b1	NM_010012	0.03	4.69E-05	24	2	60.6	250.8	224.1	172.1	160.4	92.1	75.7	47.1	51.5	74.6	80.9	122.2	134.5	207.2	165.3
Adck3	NM_001163290	0.03	4.69E-05	24	0	44.8	192.7	178.5	142.5	97.0	66.5	36.9	24.3	21.4	70.3	44.7	69.5	100.3	143.2	123.5
Pnp	NM_013632	0.03	4.69E-05	24	0	11.6	39.3	43.4	33.2	29.3	14.7	16.0	13.6	8.5	26.6	20.4	18.6	27.3	33.3	34.5
Dhcr7	NM_007856	0.03	4.69E-05	24	0	10.3	75.9	59.3	33.6	30.7	23.2	29.5	24.1	13.9	25.5	34.6	33.5	49.8	52.2	52.5
Efna1	NM_001162425	0.03	4.69E-05	24	0	8.6	44.0	29.9	25.3	25.9	17.4	19.4	9.0	12.3	24.4	15.1	31.6	27.2	41.9	26.6
Nr1d1	NM_145434	0.03	4.69E-05	24	10	7.0	1.3	1.3	20.9	8.1	32.1	18.8	6.8	9.2	5.6	2.0	0.7	0.8	1.5	0.8
Caprin1	NM_001111290	0.03	4.69E-05	24	0	6.3	30.6	24.1	19.0	13.9	10.1	9.5	7.6	5.9	18.6	15.5	17.9	18.0	22.7	22.9
Gale	NM_178389	0.03	4.69E-05	24	0	5.1	21.9	16.3	9.8	8.2	2.8	5.1	1.9	2.2	8.2	10.9	12.4	11.0	12.1	10.9
Avpr1a	NM_016847	0.03	4.69E-05	24	0	5.0	22.8	20.0	12.6	10.7	7.8	5.0	3.0	1.6	9.8	6.2	7.3	12.1	16.3	14.8
Asb13	NM_178283	0.03	4.69E-05	24	0	4.7	20.5	20.2	14.3	11.4	7.7	7.4	5.5	5.7	12.3	8.4	10.9	12.6	16.1	12.9
Mmab	NM_029956	0.03	4.69E-05	24	0	3.0	11.5	10.0	7.5	5.1	5.1	3.5	3.0	3.0	5.2	4.3	7.8	7.3	5.6	9.1
Rfxank	NM_001025589	0.03	4.69E-05	24	0	2.7	9.0	7.4	5.7	6.7	2.2	2.5	2.4	1.9	5.7	3.6	6.7	6.4	9.3	7.8
Lgalsl	NM_173752	0.03	4.69E-05	24	0	2.6	10.8	6.4	5.0	4.4	1.5	1.2	0.7	0.5	5.5	3.2	5.2	6.7	7.2	6.7
Chka	NM_013490	0.03	4.69E-05	24	0	2.5	7.7	6.3	4.8	5.0	1.3	1.5	0.2	0.5	3.6	2.0	2.3	4.6	6.3	5.8
Camk1d	NM_177343	0.03	4.69E-05	24	2	1.2	6.6	4.2	3.8	3.3	2.3	2.6	2.5	0.9	0.8	1.2	2.9	2.8	6.1	5.1
Per2	NM_011066	0.03	4.69E-05	24	18	1.2	2.8	1.5	0.7	0.2	1.3	1.2	2.0	2.0	6.6	4.8	3.2	2.8	2.1	1.6
St5	NM_001001326	0.03	4.69E-05	24	0	0.8	2.1	2.6	1.9	1.4	0.8	0.7	0.3	0.3	1.3	1.0	1.4	1.9	2.2	1.5
Dus2	NM_025518	0.03	4.69E-05	24	2	0.6	3.5	2.6	2.5	2.5	0.7	1.8	1.5	1.4	2.0	1.8	2.2	2.2	3.8	3.4
Slc34a2	NM_011402	0.03	4.69E-05	24	0	0.6	5.4	3.0	0.6	0.8	0.0	0.2	0.0	0.0	1.1	0.2	0.4	1.3	2.3	2.6
Ccdc151	NM_001163787	0.03	4.69E-05	24	20	0.3	0.7	0.7	0.6	0.3	0.1	0.3	0.7	0.3	1.6	0.8	0.7	1.0	0.7	0.7
Cyb5b	NM_025558	0.03	1.07E-04	24	0	50.9	283.6	239.2	169.2	130.8	106.1	82.4	75.6	67.5	149.0	97.2	126.9	148.2	194.2	173.6
Eif4ebp3	NM_201256	0.03	1.07E-04	24	18	43.8	97.9	75.0	30.9	24.6	53.1	18.2	187.2	100.8	396.5	111.1	92.3	110.7	56.6	64.6
Gys2	NM_145572	0.03	1.07E-04	24	16	22.4	45.8	41.6	31.0	21.7	58.8	36.8	85.5	70.9	103.3	86.3	40.5	53.7	39.0	36.6
Nop10	NM_025403	0.03	1.07E-04	24	0	19.1	197.0	170.9	123.8	122.5	107.9	102.6	86.0	95.2	188.9	115.7	129.7	135.0	147.9	135.6
Mrap	NM_029844	0.03	1.07E-04	24	0	13.4	54.0	47.0	33.6	24.9	16.4	14.5	12.6	12.1	35.3	19.3	35.4	28.4	33.3	41.7
Acss2	NM_019811	0.03	1.07E-04	24	0	12.6	80.3	62.4	36.2	21.1	23.1	16.3	18.3	13.5	26.8	25.7	30.0	58.4	53.5	48.8

Ppp1r3c	NM_016854	0.03	1.07E-04	24	1	10.7	77.1	39.5	25.9	24.0	12.0	11.7	11.1	4.3	18.4	9.5	19.5	38.5	62.1	56.4
Sgpl1	NM_009163	0.03	1.07E-04	24	0	7.1	30.3	22.3	21.8	15.8	13.2	11.6	9.9	6.8	19.6	17.6	15.9	21.8	24.8	25.0
Hypk	NM_026318	0.03	1.07E-04	24	0	7.0	62.3	58.0	28.7	33.7	31.7	27.0	19.0	22.6	34.5	33.4	42.5	36.9	39.9	35.7
Pter	NM_008961	0.03	1.07E-04	24	2	5.8	28.1	24.0	22.0	17.4	13.2	15.0	10.6	7.3	16.9	12.5	15.9	20.7	28.6	21.5
Tfpi2	NM_009364	0.03	1.07E-04	24	0	5.8	34.1	31.4	21.1	20.7	13.0	16.8	12.2	8.3	17.0	14.4	12.3	25.8	27.0	29.7
Slc16a1	NM_009196	0.03	1.07E-04	24	0	5.5	33.5	25.6	16.4	14.3	10.0	11.4	8.3	8.2	20.8	14.6	14.5	20.8	21.6	21.1
Tgm2	NM_009373	0.03	1.07E-04	24	0	5.4	58.5	37.5	25.8	20.6	18.1	16.3	13.1	10.9	24.7	24.1	24.2	23.2	35.4	27.5
Btg1	NM_007569	0.03	1.07E-04	24	0	5.1	16.9	16.3	11.4	7.9	6.0	5.1	3.6	2.8	9.5	3.3	6.3	12.3	12.6	13.5
Cdkn1a	NM_001111099	0.03	1.07E-04	24	0	3.9	22.0	14.0	4.5	5.7	0.4	2.3	0.5	0.6	6.6	2.6	7.8	5.7	7.6	12.4
Spryd7	NM_025697	0.03	1.07E-04	24	0	3.7	20.5	16.4	13.5	9.2	8.6	8.2	7.2	7.5	14.5	9.2	15.0	12.4	14.7	13.8
Acacb	NM_133904	0.03	1.07E-04	24	0	3.7	17.5	13.0	6.8	4.8	2.8	2.7	3.9	2.7	5.9	4.7	8.5	13.7	12.7	10.7
Pi4k2a	NM_145501	0.03	1.07E-04	24	0	3.4	17.6	16.8	14.7	10.8	8.4	8.1	5.6	7.3	13.7	9.4	10.5	12.0	15.6	14.0
Lsr	NM_001164185	0.03	1.07E-04	24	0	2.8	14.7	11.8	5.8	7.9	4.8	5.3	4.2	4.7	10.8	6.2	9.5	8.1	11.9	10.2
Ddx17	NM_001040187	0.03	1.07E-04	24	0	2.3	17.6	10.2	8.4	6.9	4.8	5.1	4.5	3.4	7.8	7.0	7.4	8.2	13.3	11.5
Ext2	NM_010163	0.03	1.07E-04	24	0	1.5	9.1	10.2	5.9	4.8	4.6	3.7	3.1	3.0	5.9	3.4	5.8	5.2	6.6	7.0
Ncoa5	NM_144892	0.03	1.07E-04	24	0	1.0	5.3	3.9	2.3	1.9	1.4	1.3	0.9	1.0	3.5	2.0	2.1	2.8	3.6	4.1
Atg7	NM_001253717	0.03	1.07E-04	24	0	0.9	6.0	5.5	4.1	3.4	2.8	2.5	2.1	2.2	4.0	3.4	3.5	3.1	4.8	4.4
Slc17a8	NM_182959	0.03	1.07E-04	24	0	0.9	3.3	3.1	2.2	1.1	0.9	0.5	0.3	0.9	1.3	1.4	2.2	1.7	2.3	1.7
Agpat5	NM_026792	0.03	1.07E-04	24	0	0.9	6.0	7.4	3.7	4.2	3.0	3.4	1.4	2.5	5.1	4.1	4.0	4.6	5.4	5.7
Rbmx	NM_001166623	0.03	1.07E-04	24	0	0.8	4.0	2.9	2.3	1.5	1.4	1.5	0.7	1.1	2.2	1.1	2.3	2.7	3.2	2.5
Dut	NM_023595	0.03	1.07E-04	24	0	0.5	5.5	4.2	2.2	2.5	2.6	2.0	0.7	1.1	2.0	2.0	5.4	2.6	3.3	3.1
Mthfr	NM_001161798	0.03	1.07E-04	24	2	0.4	1.6	1.0	1.0	0.9	0.2	0.2	0.0	0.1	0.8	0.4	0.5	0.8	1.6	1.2
Per3	NM_011067	0.03	1.07E-04	24	16	0.4	0.1	0.2	0.0	0.0	0.5	0.4	1.4	0.8	1.0	0.9	0.5	0.3	0.2	0.2
Oma1	NM_025909	0.03	1.07E-04	24	0	0.3	8.6	7.6	5.2	5.1	5.1	4.9	3.3	2.6	6.6	4.9	5.4	6.0	6.4	6.0
Mtrf1	NM_145960	0.03	1.07E-04	24	0	0.3	2.8	2.4	2.0	2.1	1.4	1.2	1.9	1.2	1.9	1.7	2.1	2.0	2.3	2.5
St5	NM_029811	0.03	1.07E-04	24	2	0.2	0.3	0.4	0.1	0.2	0.1	0.1	0.0	0.0	0.1	0.0	0.4	0.2	0.4	0.4
Plekhg1	NM_001033253	0.03	1.07E-04	24	0	0.1	0.8	0.8	0.5	0.6	0.4	0.3	0.5	0.3	0.5	0.5	0.6	0.6	0.7	0.7
Eif2ak4	NM_013719	0.03	1.07E-04	24	0	0.1	0.5	0.6	0.2	0.2	0.1	0.1	0.1	0.1	0.3	0.2	0.5	0.3	0.4	0.3
Creb3l1	NM_011957	0.03	1.07E-04	24	0	0.1	0.4	0.6	0.2	0.2	0.1	0.1	0.1	0.1	0.3	0.2	0.2	0.3	0.3	0.3
Prdm10	NM_001080817	0.03	1.07E-04	24	0	0.1	0.5	0.6	0.3	0.4	0.4	0.3	0.2	0.2	0.3	0.3	0.4	0.4	0.5	0.4
Bhmt	NM_016668	0.05	2.29E-04	24	0	57.1	362.2	255.4	289.4	185.9	124.4	119.1	114.4	86.9	175.5	136.1	138.8	248.3	245.3	318.2
Plin2	NM_007408	0.05	2.29E-04	24	2	46.8	236.4	188.9	145.4	159.6	137.3	93.5	56.2	66.7	118.5	90.0	106.9	141.7	195.0	145.1
S100a10	NM_009112	0.05	2.29E-04	24	0	42.9	251.9	240.6	210.9	169.6	110.4	111.9	94.9	66.3	153.0	110.9	128.9	160.6	191.6	193.6
Cyb5r3	NM_029787	0.05	2.29E-04	24	0	35.4	317.2	278.3	210.4	187.7	184.2	160.3	157.6	146.6	258.5	188.5	190.8	233.0	253.0	235.9
Sdc1	NM_011519	0.05	2.29E-04	24	0	33.1	203.0	165.9	96.1	85.7	60.3	47.8	63.9	46.1	144.9	71.1	107.8	105.6	129.4	117.2
Tubb2a	NM_009450	0.05	2.29E-04	24	0	29.5	79.5	60.2	51.5	36.8	5.7	9.8	4.8	2.4	37.9	17.9	27.2	39.2	83.6	51.2
Ddc	NM_001190448	0.05	2.29E-04	24	0	19.3	81.0	59.3	45.5	47.0	18.4	22.2	13.2	12.9	54.8	37.3	43.1	56.8	52.4	55.4
Gclc	NM_010295	0.05	2.29E-04	24	2	16.2	66.9	71.1	60.3	51.2	44.5	29.1	26.7	23.5	35.5	28.3	31.7	44.7	63.3	54.3
Tars	NM_033074	0.05	2.29E-04	24	0	15.6	62.1	52.9	43.9	33.1	20.1	18.8	14.3	12.7	35.3	27.6	26.4	40.9	49.9	40.4
Pnkd	NM_001039509	0.05	2.29E-04	24	0	12.5	46.8	41.1	32.1	22.8	14.5	9.8	9.1	6.7	30.0	14.6	21.8	25.1	35.1	26.7
Hmgcs1	NM_145942	0.05	2.29E-04	24	0	11.2	62.0	58.9	37.6	26.4	23.5	41.8	16.9	10.5	25.0	21.7	31.3	56.0	57.4	54.0
Cldn2	NM_016675	0.05	2.29E-04	24	0	11.0	49.0	42.0	35.3	31.6	20.9	19.7	14.2	16.8	32.8	20.6	19.7	37.2	38.8	35.5
Acsl4	NM_001033600	0.05	2.29E-04	24	20	10.4	31.2	26.2	18.7	17.0	14.2	16.6	23.7	16.2	31.7	35.1	30.2	38.0	29.8	27.1
Adh4	NM_011996	0.05	2.29E-04	24	2	9.8	57.5	58.3	51.4	43.1	43.5	42.5	32.3	22.4	42.4	37.5	30.9	51.7	58.5	64.0
Ran	NM_009391	0.05	2.29E-04	24	0	8.6	63.1	52.5	34.4	25.9	21.7	23.6	20.5	21.5	36.9	28.7	26.9	33.8	50.7	38.4
Fdft1	NM_010191	0.05	2.29E-04	24	0	6.2	22.9	21.4	7.1	7.5	6.6	13.6	6.4	4.2	10.7	11.3	15.4	17.9	19.6	18.6
Mal2	NM_178920	0.05	2.29E-04	24	0	5.7	24.9	24.0	11.4	9.4	5.8	4.8	4.2	6.9	22.2	9.2	14.9	13.8	17.8	18.0
Atg101	NM_026566	0.05	2.29E-04	24	0	5.4	28.0	24.8	20.2	16.7	12.8	11.9	7.2	8.3	18.9	11.0	13.9	17.0	22.8	21.1
2610528J11Rik	NM_025572	0.05	2.29E-04	24	0	4.9	16.4	16.6	13.3	9.9	10.3	5.5	5.4	3.6	9.4	6.4	7.9	11.6	13.5	14.1
Lpin1	NM_001130412	0.05	2.29E-04	24	15	4.3	3.8	3.6	2.7	1.9	7.2	7.3	66.9	50.2	17.8	15.8	5.1	4.0	3.4	2.8
Ubqln1	NM_152234	0.05	2.29E-04	24	0	3.9	29.4	29.1	21.9	19.8	16.6	14.5	14.1	12.6	28.3	18.5	21.0	21.0	25.9	23.5
Nmrk1	NM_145497	0.05	2.29E-04	24	18	3.9	6.0	5.5	3.5	4.3	3.9	3.4	14.9	9.5	16.2	11.6	7.0	7.2	4.5	5.5
Anp32a	NM_009672	0.05	2.29E-04	24	0	3.4	39.8	39.6	29.9	21.8	20.0	17.0	19.8	15.4	21.0	20.0	17.3	31.3	37.0	32.9
Ppm1b	NM_001159496	0.05	2.29E-04	24	0	2.9	16.6	16.0	13.9	9.3	10.3	7.2	8.3	5.6	12.5	8.9	11.1	11.7	15.7	14.5
Tnfaip2	NM_009396	0.05	2.29E-04	24	1	2.8	10.6	8.3	7.3	6.6	4.0	2.8	2.5	1.4	4.3	2.6	4.7	5.7	8.0	6.4
Tlcd1	NM_026708	0.05	2.29E-04	24	18	2.7	7.5	4.4	4.9	3.9	6.0	5.0	8.1	6.4	10.6	8.7	9.0	8.4	7.1	6.2

Pabpn1	NM_019402	0.05	2.29E-04	24	0	2.6	15.8	14.0	10.4	8.2	7.5	6.8	5.5	5.6	12.6	7.6	9.5	13.2	13.2	8.6
Tspan33	NM_146173	0.05	2.29E-04	24	0	2.3	9.3	8.4	7.2	5.7	4.6	3.7	3.6	3.1	5.6	3.5	6.7	5.0	7.0	8.0
Acnat1	NM_001164565	0.05	2.29E-04	24	0	2.1	11.9	10.6	7.1	6.3	4.9	3.7	3.3	2.3	7.8	6.8	4.9	7.9	10.9	8.0
40057	NM_001113487	0.05	2.29E-04	24	0	2.1	11.8	10.4	7.7	6.8	5.2	4.3	3.3	2.3	7.9	6.4	8.1	7.7	9.1	7.3
Lpin2	NM_022882	0.05	2.29E-04	24	14	2.1	4.4	4.9	3.6	3.8	6.8	5.6	10.9	8.6	8.9	7.8	4.9	5.4	4.0	2.9
Mtap	NM_024433	0.05	2.29E-04	24	0	2.0	16.0	14.0	7.4	7.6	6.5	6.1	5.6	4.8	11.2	6.1	7.8	10.2	10.1	13.9
Taf15	NM_027427	0.05	2.29E-04	24	0	1.7	17.6	14.4	8.6	6.8	6.1	7.2	8.0	5.6	9.2	8.6	9.6	10.4	13.6	9.6
Rpa1	NM_001164223	0.05	2.29E-04	24	0	1.5	11.6	10.2	8.1	6.3	5.0	6.2	5.4	4.6	6.0	6.9	6.0	7.7	9.5	8.3
Lnx2	NM_080795	0.05	2.29E-04	24	0	1.4	7.3	6.8	3.8	3.7	2.1	2.1	1.3	1.5	6.5	3.2	4.1	3.4	5.9	4.3
Gca	NM_145523	0.05	2.29E-04	24	0	1.2	3.6	5.4	2.9	2.5	1.3	1.5	0.1	1.2	2.3	2.3	3.1	2.5	2.0	4.0
Bco2	NM_133217	0.05	2.29E-04	24	0	1.1	6.2	6.3	4.2	3.3	4.1	2.7	1.9	1.7	3.0	2.8	2.9	4.6	5.8	4.5
Itgb5	NM_001145884	0.05	2.29E-04	24	0	0.9	8.4	6.8	4.1	4.5	3.4	2.8	3.2	2.2	4.8	3.4	3.5	4.8	6.4	5.2
Sorbs2	NM_001205219	0.05	2.29E-04	24	0	0.9	5.1	4.3	3.9	3.9	3.0	3.2	2.0	1.7	4.6	3.3	4.1	4.8	5.0	4.2
Arntl	NM_007489	0.05	2.29E-04	24	0	0.9	2.3	2.9	2.1	1.2	0.2	0.2	0.3	0.0	0.7	0.8	1.0	1.5	2.1	1.0
40787	NM_001009818	0.05	2.29E-04	24	0	0.7	5.0	4.3	3.2	2.3	1.9	2.2	1.6	1.1	2.4	4.4	3.2	3.3	3.4	4.0
Shkbp1	NM_138676	0.05	2.29E-04	24	0	0.7	2.7	2.3	1.7	1.5	1.1	0.9	1.0	0.9	1.7	1.1	2.1	1.6	2.0	1.7
Syne1	NM_001079686	0.05	2.29E-04	24	4	0.5	1.4	1.8	2.1	1.5	1.1	0.8	0.6	0.3	0.6	0.5	0.6	1.0	1.8	1.7
Rad9a	NM_011237	0.05	2.29E-04	24	22	0.5	1.4	1.1	0.6	0.6	0.1	0.2	0.3	0.3	0.8	0.7	1.0	1.0	1.3	0.7
Smarcal1	NM_018817	0.05	2.29E-04	24	0	0.4	3.5	3.3	2.3	2.1	1.7	1.5	0.9	1.0	2.0	2.1	1.9	2.1	2.8	2.3
Gtf3c5	NM_148928	0.05	2.29E-04	24	0	0.4	3.9	2.5	1.8	1.8	1.4	1.4	0.7	1.1	1.6	1.4	1.4	2.2	2.4	1.7
Ptpn9	NM_019651	0.05	2.29E-04	24	0	0.3	3.3	2.3	1.3	1.6	0.8	1.1	1.0	1.1	1.9	1.1	1.3	2.3	2.1	2.9
Ddhd1	NM_001039106	0.05	2.29E-04	24	0	0.3	2.1	1.9	0.9	1.0	0.6	0.6	0.8	0.5	1.4	0.8	0.9	1.1	1.5	1.4
E4f1	NM_007893	0.05	2.29E-04	24	0	0.3	1.3	0.9	0.6	0.6	0.4	0.5	0.4	0.3	0.8	0.5	1.0	0.8	1.1	0.7
Sorbs2	NM_172752	0.05	2.29E-04	24	0	0.2	2.2	2.6	1.8	1.4	1.4	1.6	0.9	0.9	1.7	1.5	1.5	2.0	2.0	2.1
Opn3	NM_010098	0.05	2.29E-04	24	0	0.1	0.8	0.6	0.1	0.2	0.1	0.2	0.0	0.0	0.3	0.1	0.2	0.3	0.4	0.5

Supplementary Table 2 | JTK analysis of ribosome profiling data for circadian (BH.Q < 0.05) transcripts.

References

Akhtar, R.A., Reddy, A.B., Maywood, E.S., Clayton, J.D., King, V.M., Smith, A.G., Gant, T.W., Hastings, M.H., and Kyriacou, C.P. (2002). Circadian cycling of the mouse liver transcriptome, as revealed by cDNA microarray, is driven by the suprachiasmatic nucleus. Curr. Biol. CB *12*, 540–550. .

Atger, F., Gobet, C., Marquis, J., Martin, E., Wang, J., Weger, B., Lefebvre, G., Descombes, P., Naef, F., and Gachon, F. (2015). Circadian and feeding rhythms differentially affect rhythmic mRNA transcription and translation in mouse liver. Proc. Natl. Acad. Sci. U. S. A. *112*, E6579-6588. https://doi.org/10.1073/pnas.1515308112.

Bohlen, J., Harbrecht, L., Blanco, S., Clemm von Hohenberg, K., Fenzl, K., Kramer, G., Bukau, B., and Teleman, A.A. (2020). DENR promotes translation reinitiation via ribosome recycling to drive expression of oncogenes including ATF4. Nat. Commun. *11*, 4676. https://doi.org/10.1038/s41467-020-18452-2.

Castelo-Szekely, V., Arpat, A.B., Janich, P., and Gatfield, D. (2017). Translational contributions to tissue specificity in rhythmic and constitutive gene expression. Genome Biol. *18*, 116. https://doi.org/10.1186/s13059-017-1222-2.

Chen, R., Schirmer, A., Lee, Y., Lee, H., Kumar, V., Yoo, S.-H., Takahashi, J.S., and Lee, C. (2009). Rhythmic PER abundance defines a critical nodal point for negative feedback within the circadian clock mechanism. Mol. Cell *36*, 417–430. https://doi.org/10.1016/j.molcel.2009.10.012.

Chew, G.-L., Pauli, A., and Schier, A.F. (2016). Conservation of uORF repressiveness and sequence features in mouse, human and zebrafish. Nat. Commun. *7*, 11663. https://doi.org/10.1038/ncomms11663.

Dacheux, E., Malys, N., Meng, X., Ramachandran, V., Mendes, P., and McCarthy, J.E. (2017). Translation initiation events on structured eukaryotic mRNAs generate gene expression noise. Nucleic Acids Res. *45*, 6981–6992. https://doi.org/10.1093/nar/gkx430.

Diernfellner, A.C.R., Schafmeier, T., Merrow, M.W., and Brunner, M. (2005). Molecular mechanism of temperature sensing by the circadian clock of Neurospora crassa. Genes Dev. *19*, 1968–1973. https://doi.org/10.1101/gad.345905.

Doi, M., Shimatani, H., Atobe, Y., Murai, I., Hayashi, H., Takahashi, Y., Fustin, J.-M., Yamaguchi, Y., Kiyonari, H., Koike, N., et al. (2019). Non-coding cis -element of Period2 is essential for maintaining organismal circadian behaviour and body temperature rhythmicity. Nat. Commun. *10*, 2563. https://doi.org/10.1038/s41467-019-10532-2.

Everett, L.J., and Lazar, M.A. (2014). Nuclear Receptor Rev-erbα: Up, Down, and All Around. Trends Endocrinol. Metab. TEM *25*, 586–592. https://doi.org/10.1016/j.tem.2014.06.011.

Feng, D., Liu, T., Sun, Z., Bugge, A., Mullican, S.E., Alenghat, T., Liu, X.S., and Lazar, M.A. (2011). A circadian rhythm orchestrated by histone deacetylase 3 controls hepatic lipid metabolism. Science *331*, 1315–1319. https://doi.org/10.1126/science.1198125.

Field, M.D., Maywood, E.S., O'Brien, J.A., Weaver, D.R., Reppert, S.M., and Hastings, M.H. (2000). Analysis of clock proteins in mouse SCN demonstrates phylogenetic divergence of the circadian clockwork and resetting mechanisms. Neuron *25*, 437–447. .

Gekakis, N., Staknis, D., Nguyen, H.B., Davis, F.C., Wilsbacher, L.D., King, D.P., Takahashi, J.S., and Weitz, C.J. (1998). Role of the CLOCK Protein in the Mammalian Circadian Mechanism. Science *280*, 1564–1569. https://doi.org/10.1126/science.280.5369.1564.

Gygi, S.P., Rochon, Y., Franza, B.R., and Aebersold, R. (1999). Correlation between Protein and mRNA Abundance in Yeast. Mol. Cell. Biol. *19*, 1720–1730. https://doi.org/10.1128/MCB.19.3.1720.

Hao, H., Allen, D.L., and Hardin, P.E. (1997). A circadian enhancer mediates PER-dependent mRNA cycling in Drosophila melanogaster. Mol. Cell. Biol. *17*, 3687–3693. https://doi.org/10.1128/MCB.17.7.3687.

Honkela, A., Peltonen, J., Topa, H., Charapitsa, I., Matarese, F., Grote, K., Stunnenberg, H.G., Reid, G., Lawrence, N.D., and Rattray, M. (2015). Genome-wide modeling of transcription kinetics reveals patterns of RNA production delays. Proc. Natl. Acad. Sci. U. S. A. *112*, 13115–13120. https://doi.org/10.1073/pnas.1420404112.

Hughes, M.E., Hogenesch, J.B., and Kornacker, K. (2010). JTK_CYCLE: an efficient nonparametric algorithm for detecting rhythmic components in genome-scale data sets. J. Biol. Rhythms *25*, 372–380. https://doi.org/10.1177/0748730410379711.

Hunter, A.L., Pelekanou, C.E., Adamson, A., Downton, P., Barron, N.J., Cornfield, T., Poolman, T.M., Humphreys, N., Cunningham, P.S., Hodson, L., et al. (2020). Nuclear receptor REVERBα is a state-dependent regulator of liver energy metabolism. Proc. Natl. Acad. Sci. U. S. A. *117*, 25869–25879. https://doi.org/10.1073/pnas.2005330117.

Ingolia, N.T., Brar, G.A., Rouskin, S., McGeachy, A.M., and Weissman, J.S. (2012). The ribosome profiling strategy for monitoring translation in vivo by deep sequencing of ribosome-protected mRNA fragments. Nat. Protoc. *7*, 1534–1550. https://doi.org/10.1038/nprot.2012.086.

Isojima, Y., Nakajima, M., Ukai, H., Fujishima, H., Yamada, R.G., Masumoto, K., Kiuchi, R., Ishida, M., Ukai-Tadenuma, M., Minami, Y., et al. (2009). CKIε/δ-dependent phosphorylation is a temperature-insensitive, period-determining process in the mammalian circadian clock. Proc. Natl. Acad. Sci. https://doi.org/10.1073/pnas.0908733106.

Jang, C., Lahens, N.F., Hogenesch, J.B., and Sehgal, A. (2015). Ribosome profiling reveals an important role for translational control in circadian gene expression. Genome Res. *25*, 1836–1847. https://doi.org/10.1101/gr.191296.115.

Janich, P., Arpat, A.B., Castelo-Szekely, V., Lopes, M., and Gatfield, D. (2015). Ribosome profiling reveals the rhythmic liver translatome and circadian clock regulation by upstream open reading frames. Genome Res. *25*, 1848–1859. https://doi.org/10.1101/gr.195404.115.

Johnstone, T.G., Bazzini, A.A., and Giraldez, A.J. (2016). Upstream ORFs are prevalent translational repressors in vertebrates. EMBO J. *35*, 706–723. https://doi.org/10.15252/embj.201592759.

Koike, N., Yoo, S.-H., Huang, H.-C., Kumar, V., Lee, C., Kim, T.-K., and Takahashi, J.S. (2012). Transcriptional architecture and chromatin landscape of the core circadian clock in mammals. Science *338*, 349–354. https://doi.org/10.1126/science.1226339.

Kojima, S., Shingle, D.L., and Green, C.B. (2011). Post-transcriptional control of circadian rhythms. J. Cell Sci. *124*, 311–320. https://doi.org/10.1242/jcs.065771.

Langmead, B., and Salzberg, S.L. (2012). Fast gapped-read alignment with Bowtie 2. Nat. Methods *9*, 357–359. https://doi.org/10.1038/nmeth.1923.

Lee, C., Etchegaray, J.P., Cagampang, F.R., Loudon, A.S., and Reppert, S.M. (2001). Posttranslational mechanisms regulate the mammalian circadian clock. Cell *107*, 855–867. .

Lim, C., and Allada, R. (2013). Emerging roles for post-transcriptional regulation in circadian clocks. Nat. Neurosci. *16*, 1544–1550. https://doi.org/10.1038/nn.3543.

Liu, Y., Beyer, A., and Aebersold, R. (2016). On the Dependency of Cellular Protein Levels on mRNA Abundance. Cell *165*, 535–550. https://doi.org/10.1016/j.cell.2016.03.014.

Mauvoisin, D., Wang, J., Jouffe, C., Martin, E., Atger, F., Waridel, P., Quadroni, M., Gachon, F., and Naef, F. (2014). Circadian clock-dependent and -independent rhythmic proteomes implement distinct diurnal functions in mouse liver. Proc. Natl. Acad. Sci. U. S. A. *111*, 167–172. https://doi.org/10.1073/pnas.1314066111.

Millius, A., and Ueda, H.R. (2017). Systems Biology-Derived Discoveries of Intrinsic Clocks. Front. Neurol. *8*, 25. https://doi.org/10.3389/fneur.2017.00025.

Mohawk, J.A., Green, C.B., and Takahashi, J.S. (2012). Central and peripheral circadian clocks in mammals. Annu. Rev. Neurosci. *35*, 445–462. https://doi.org/10.1146/annurev-neuro-060909-153128.

Morris, D.R., and Geballe, A.P. (2000). Upstream open reading frames as regulators of mRNA translation. Mol. Cell. Biol. *20*, 8635–8642. https://doi.org/10.1128/mcb.20.23.8635-8642.2000.

Mosig, R.A., Castaneda, A.N., Deslauriers, J.C., Frazier, L.P., He, K.L., Maghzian, N., Pokharel, A., Schrier, C.T., Zhu, L., Koike, N., et al. (2020). Natural Antisense Transcript of Period2, Per2AS, regulates the amplitude of the mouse circadian clock. BioRxiv 2020.07.27.222760. https://doi.org/10.1101/2020.07.27.222760.

Mosig, R.A., Castaneda, A.N., Deslauriers, J.C., Frazier, L.P., He, K.L., Maghzian, N., Pokharel, A., Schrier, C.T., Zhu, L., Koike, N., et al. (2021). Natural antisense transcript of Period2, Per2AS, regulates the amplitude of the mouse circadian clock. Genes Dev. *35*, 899–913. https://doi.org/10.1101/gad.343541.120.

Moškon, M. (2020). CosinorPy: a python package for cosinor-based rhythmometry. BMC Bioinformatics *21*, 485. https://doi.org/10.1186/s12859-020-03830-w.

Nagel, R., Clijsters, L., and Agami, R. (2009). The miRNA-192/194 cluster regulates the Period gene family and the circadian clock. FEBS J. *276*, 5447–5455. https://doi.org/10.1111/j.1742-4658.2009.07229.x.

Narumi, R., Shimizu, Y., Ukai-Tadenuma, M., Ode, K.L., Kanda, G.N., Shinohara, Y., Sato, A., Matsumoto, K., and Ueda, H.R. (2016). Mass spectrometry-based absolute quantification reveals rhythmic variation of mouse circadian clock proteins. Proc. Natl. Acad. Sci. U. S. A. *113*, E3461-3467. https://doi.org/10.1073/pnas.1603799113.

Okamoto-Uchida, Y., Izawa, J., Nishimura, A., Hattori, A., Suzuki, N., and Hirayama, J. (2019). Post-translational Modifications are Required for Circadian Clock Regulation in Vertebrates. Curr. Genomics *20*, 332–339. https://doi.org/10.2174/1389202919666191014094349.

Park, I., Kim, D., Kim, J., Jang, S., Choi, M., Choe, H.K., Choe, Y., and Kim, K. (2020). microRNA-25 as a novel modulator of circadian Period2 gene oscillation. Exp. Mol. Med. *52*, 1614–1626. https://doi.org/10.1038/s12276-020-00496-5.

Ran, F.A., Hsu, P.D., Wright, J., Agarwala, V., Scott, D.A., and Zhang, F. (2013). Genome engineering using the CRISPR-Cas9 system. Nat. Protoc. *8*, 2281–2308. https://doi.org/10.1038/nprot.2013.143.

Reddy, A.B., Karp, N.A., Maywood, E.S., Sage, E.A., Deery, M., O'Neill, J.S., Wong, G.K.Y., Chesham, J., Odell, M., Lilley, K.S., et al. (2006). Circadian orchestration of the hepatic proteome. Curr. Biol. CB *16*, 1107–1115. https://doi.org/10.1016/j.cub.2006.04.026.

Robles, M.S., Cox, J., and Mann, M. (2014). In-vivo quantitative proteomics reveals a key contribution of post-transcriptional mechanisms to the circadian regulation of liver metabolism. PLoS Genet. *10*, e1004047. https://doi.org/10.1371/journal.pgen.1004047.

Robles, M.S., Humphrey, S.J., and Mann, M. (2017). Phosphorylation Is a Central Mechanism for Circadian Control of Metabolism and Physiology. Cell Metab. *25*, 118–127. https://doi.org/10.1016/j.cmet.2016.10.004.

Sato, T.K., Yamada, R.G., Ukai, H., Baggs, J.E., Miraglia, L.J., Kobayashi, T.J., Welsh, D.K., Kay, S.A., Ueda, H.R., and Hogenesch, J.B. (2006). Feedback repression is required for mammalian circadian clock function. Nat. Genet. *38*, 312–319. https://doi.org/10.1038/ng1745.

Schleich, S., Strassburger, K., Janiesch, P.C., Koledachkina, T., Miller, K.K., Haneke, K., Cheng, Y.-S., Küchler, K., Stoecklin, G., Duncan, K.E., et al. (2014). DENR-MCT-1 promotes translation re-initiation downstream of uORFs to control tissue growth. Nature *512*, 208–212. https://doi.org/10.1038/nature13401.

Shimizu, Y., Inoue, A., Tomari, Y., Suzuki, T., Yokogawa, T., Nishikawa, K., and Ueda, T. (2001). Cell-free translation reconstituted with purified components. Nat. Biotechnol. *19*, 751–755. https://doi.org/10.1038/90802.

Sunagawa, G.A., Sumiyama, K., Ukai-Tadenuma, M., Perrin, D., Fujishima, H., Ukai, H., Nishimura, O., Shi, S., Ohno, R., Narumi, R., et al. (2016). Mammalian Reverse Genetics without Crossing Reveals Nr3a as a Short-Sleeper Gene. Cell Rep. *14*, 662–677. https://doi.org/10.1016/j.celrep.2015.12.052.

Tatsuki, F., Sunagawa, G.A., Shi, S., Susaki, E.A., Yukinaga, H., Perrin, D., Sumiyama, K., Ukai-Tadenuma, M., Fujishima, H., Ohno, R., et al. (2016). Involvement of Ca(2+)-Dependent Hyperpolarization in Sleep Duration in Mammals. Neuron *90*, 70–85. https://doi.org/10.1016/j.neuron.2016.02.032.

Ueda, H.R., Hayashi, S., Chen, W., Sano, M., Machida, M., Shigeyoshi, Y., Iino, M., and Hashimoto, S. (2005). System-level identification of transcriptional circuits underlying mammalian circadian clocks. Nat. Genet. *37*, 187–192. https://doi.org/10.1038/ng1504.

Ukai-Tadenuma, M., Yamada, R.G., Xu, H., Ripperger, J.A., Liu, A.C., and Ueda, H.R. (2011). Delay in feedback repression by cryptochrome 1 is required for circadian clock function. Cell *144*, 268–281. https://doi.org/10.1016/j.cell.2010.12.019.

Wang, J., Mauvoisin, D., Martin, E., Atger, F., Galindo, A.N., Dayon, L., Sizzano, F., Palini, A., Kussmann, M., Waridel, P., et al. (2017). Nuclear Proteomics Uncovers Diurnal Regulatory Landscapes in Mouse Liver. Cell Metab. *25*, 102–117. https://doi.org/10.1016/j.cmet.2016.10.003.

Wang, Y., Song, L., Liu, M., Ge, R., Zhou, Q., Liu, W., Li, R., Qie, J., Zhen, B., Wang, Y., et al. (2018). A proteomics landscape of circadian clock in mouse liver. Nat. Commun. *9*, 1553. https://doi.org/10.1038/s41467-018-03898-2.

Woo, K.-C., Kim, T.-D., Lee, K.-H., Kim, D.-Y., Kim, W., Lee, K.-Y., and Kim, K.-T. (2009). Mouse period 2 mRNA circadian oscillation is modulated by PTB-mediated rhythmic mRNA degradation. Nucleic Acids Res. *37*, 26–37. https://doi.org/10.1093/nar/gkn893.

Wu, H.-W., Fajiculay, E., Wu, J.-F., Yan, C.-C.S., Hsu, C.-P., and Wu, S.-H. (2022). Noise reduction by upstream open reading frames. Nat. Plants *8*, 474–480. https://doi.org/10.1038/s41477-022-01136-8.

Yoo, S.-H., Yamazaki, S., Lowrey, P.L., Shimomura, K., Ko, C.H., Buhr, E.D., Siepka, S.M., Hong, H.-K., Oh, W.J., Yoo, O.J., et al. (2004). PERIOD2::LUCIFERASE real-time reporting of circadian dynamics reveals persistent circadian oscillations in mouse peripheral tissues. Proc. Natl. Acad. Sci. U. S. A. *101*, 5339–5346. https://doi.org/10.1073/pnas.0308709101.

Yoo, S.-H., Kojima, S., Shimomura, K., Koike, N., Buhr, E.D., Furukawa, T., Ko, C.H., Gloston, G., Ayoub, C., Nohara, K., et al. (2017). Period2 3’-UTR and microRNA-24 regulate circadian rhythms by repressing PERIOD2 protein accumulation. Proc. Natl. Acad. Sci. U. S. A. *114*, E8855–E8864. https://doi.org/10.1073/pnas.1706611114.

Zhang, Y., Fang, B., Emmett, M.J., Damle, M., Sun, Z., Feng, D., Armour, S.M., Remsberg, J.R., Jager, J., Soccio, R.E., et al. (2015). Discrete Functions of Nuclear Receptor Rev-erbα Couple Metabolism to the Clock. Science *348*, 1488–1492. https://doi.org/10.1126/science.aab3021.